Master's thesis

NTNU
Norwegian University of Science and Technology
Faculty of Natural Sciences
Department of Chemical Engineering

Mats Kulås

Dynamic Optimization and Parameter Estimation used on an Extrusion Press for Aluminium

Master's thesis in Industrial Chemistry and Biotechnology
Supervisor: Johannes Jäschke
Co-supervisor: Anne Øyen Halås
June 2022

NTNU
Kunnskap for en bedre verden

Mats Kulås

Dynamic Optimization and Parameter Estimation used on an Extrusion Press for Aluminium

Master's thesis in Industrial Chemistry and Biotechnology
Supervisor: Johannes Jäschke
Co-supervisor: Anne Øyen Halås
June 2022

Norwegian University of Science and Technology
Faculty of Natural Sciences
Department of Chemical Engineering

NTNU
Norwegian University of
Science and Technology

Preface

This project was undertaken as part of a master thesis at the Department of Chemical Engineering at NTNU, and it builds on work performed in a specialization project the previous semester. The work was performed the last semester of the 5 year integrated master program Industrial Chemistry and Biotechnology, and it corresponds to 20 weeks of work. It is part of a larger project called ExtruTeC, a collaboration between Hydro, Cybernetica, Sintef and NTNU, and this work was performed under the supervision of Cybernetica. The main supervisor for the project was professor Johannes Jäschke at the Department of Chemical Engineering at NTNU. M.Sc. Anne Øyen Halås from Cybernetica was co-supervisor for the project.

I would like to express my gratitude to Cybernetica for giving me the opportunity to work on this project and to Johannes Jäschke for agreeing to be my supervisor. I would especially like to thank Anne Øyen Halås for all the help and tips I have received during this project. It was especially helpful while figuring out the software used. I would also like to thank Dr.Ing. Peter Singstad and M.Sc. Fredrik Gjertsen for many helpful inputs and thoughts during our project meetings.

Trondheim, May 31, 2022
Mats Kulås

Abstract

Today aluminium is used in more and more applications, due to its high strength, low weight and cheap recyclability. Some of these uses, like the radiators in modern cars, required very precise manufacturing. The radiators benefit from using very thin walled hollow profiles produced by a process called extrusion. In this process, an aluminium cylinder called a billet is heated and then pressed through a tool, called the die, shaping it to the desired profile. For thin walled profiles, this process often results in tearing and deformation in the aluminium if the temperature is not controlled appropriately. To be able to reliably produce high quality profiles and reduce wall thickness further development of better temperature control is therefore needed.

This project was concerned with two aspects of improving the temperature control during extrusion, optimization and parameter estimation. A model of the whole system was created by combining several existing first principle models of system parts created by Cybernetica. This model was used for open loop dynamic optimization, with the aim of keeping the peak temperature during extrusion constant while performing the extrusion as fast as possible. This was done by manipulating the extrusion speed and the set points in the preheater. Parameter estimation was performed using moving horizon estimation to determine which parameters should be estimated to give accurate model predictions, and also what their initial values should be.

The optimization results showed that significant improvements in extrusion time compared to today's practice could be made while also keeping the peak temperature constant. By optimizing the preheating and extrusion speed the extrusion time was reduced by approximately 30% and no significant deviations in the peak temperature from its set point were observed. The parameter estimation showed that accurate predictions in the extrusion press were possible by only estimating two parameters, a correction factor for a heat generation term and a time constant for a heat loss term in the die. Better initial values were also found for these parameters. For the preheater model good accuracy was not achieved, indicating either a bad model fit or inaccurate measurements. For the model of the transfer of the billet from the preheater to the press it was found that there were too few measurements for accurate parameter estimation, but model predictions were still good.

Sammendrag

I dag blir aluminium brukt i flere og flere produkter. Noen av disse, som radiatoren i moderne biler, krever veldig presise produksjonsmetoder. Her brukes tynne, hule profiler som varmevekslere, og de produseres ved ekstrudering. Da blir en aluminiumsylinder, kalt en billet, forvarmet for så å bli presset gjennom et verktøy som former den til ønsket profil. For tynne profiler kan denne prosessen resultere i skader og deformering av produktet hvis ikke temperaturen er riktig. For å kunne lage slike produkter med minst mulig skader og enda tynnere vegger trenger man derfor bedre kontroll på temperaturen under ekstrudering.

Målet for dette prosjektet er å bidra til forbedret temperaturkontroll på to ulike måter, optimalisering av prosessen og parameterestimering. Til dette ble en modell for hele prosessen brukt, inkludert forvarming og transport fra forvarmet til presse. Denne modellen ble satt sammen av eksisterende modeller for hver delprosess laget av Cybernetica. Den ble så brukt i dynamisk optimalisering for å holde den høyeste temperaturen aluminiumet oppnår under ekstrudering konstant samtidig som ekstrudering ble gjennomført så fort som mulig. Dette ble gjort ved å justere pressehastigheten og forvarmingen. Parameterestimering ble utført med moving horizon estimation, og målet var å finne ut hvilke parametre som burde estimeres for å gi gode prediksjoner fra modellen, samt å finne gode initialverdier for dem.

Resultatene fra optimaliseringen viste at betydelige forbedringer er mulig sammenlignet med måten pressen driftes på i dag. Det var mulig å holde temperaturen konstant på ønsket verdi samtidig som ekstruderingstiden ble redusert med omtrent 30%. Parameterestimeringen viste at det var mulig å oppnå gode prediksjoner fra modellen i pressa ved å estimere kun to av parameterne. Disse var en korreksjonsfaktor for et varmegenerasjonsledd i modellen og tidskonstanten til et varmetapsledd i verktøyet. Bedre initialverdier ble også funnet for disse parameterne. I forvarmeren klarte ikke modellen å gi gode prediksjoner for alle målingene, noe som enten kan komme av at modellen ikke passer godt nok til systemet eller feil i målingene. I modellen for transport mellom forvarmer og presse var det for få målinger til å kunne gi gode parameterestimater, men modellens prediksjoner var likevel gode.

Contents

1 Introduction

1.1 Background

Aluminium can be found everywhere in the modern world. Due to its low weight and high strength it is used in car parts, phones, construction and many other places [11]. As society becomes more focused on sustainability and recycling, aluminium is becoming even more popular, as it can be recycled infinitely for a fraction of the production cost. Aluminium is now being used for new purposes and improvements are made the existing products. Some of the new products require improvements of production methods. For example, aluminium is now used in the radiators of electric cars. Here, thin walled hollow profiles like the ones shown in Figure 1.1 are used as heat exchangers. To ensure that these are as effective as possible, meaning that they have the highest possible heat transfer, it is desirable for them to have as thin walls as possible. This also reduces their weight, which means the car will be lighter and use less energy. Producing thinner walls is however difficult. The profiles are made using a process called extrusion, and they are prone to deformation and tearing if the extrusion press is not operated at the correct temperature. Therefore, developing accurate temperature control for the process is important. This might also allow for faster extrusion, which would increase the productivity and profitability of the extrusion presses. This project therefore aims to investigate how the extrusion presses should be operated to ensure fast operation at the right temperature using open loop dynamic optimization. In addition, values of parameters used in a model of the process will be estimated, to ensure that the model accurately can describe the real system.

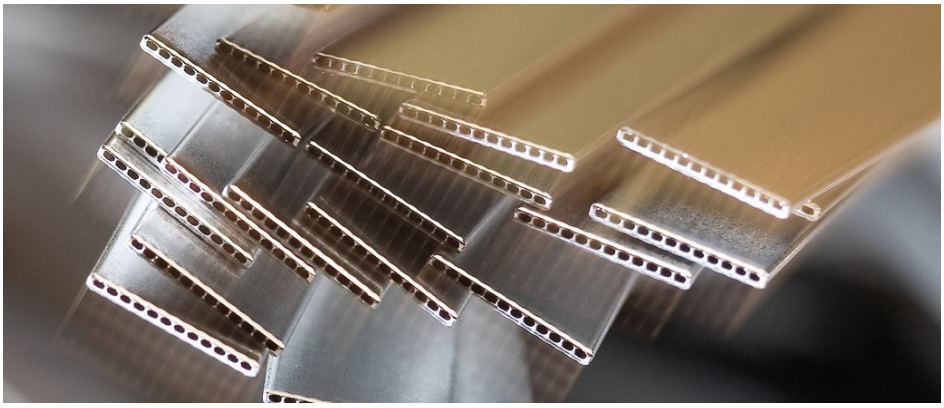

Figure 1.1: Picture of thin walled micro channel tubes from Hydro [16]

This project is a part of a larger project where Hydro, Cybernetica, Sintef and NTNU collaborate. The project is called ExtruTeC and aims to develop both model predictive control for the extrusion presses, as well as batch optimization for the extrusion cycle [18]. The work presented in this report is concerned with the batch optimization part of the main project, and existing models developed by Cybernetica are used for both dynamic optimization and parameter estimation.

1.2 Literature review

Modeling and optimization of aluminium extrusion has been investigated in several previous studies. Models have mostly been based on finite elements, and optimization has been performed to keep the peak temperature during extrusion constant and in the desired range. Less has been published on state and parameter estimation for extrusion, but several studies have investigated methods for estimation on other constrained nonlinear systems. As the extrusion process is both constrained and nonlinear their findings are expected to be relevant for this process as well.

Matamoros[9] developed both a model for an aluminium extrusion process and nonlinear model predictive control for use in temperature control of the process. The model was semi-analytical, as the equation of energy was solved using finite elements while the equations of continuity and motion were solved analytically. This approach significantly reduced the computational load compared to models solving all three equations using finite elements, and the model was still able to accurately describe the process. Simulations with the model predictive controller showed that good temperature control was possible by adjusting how fast the aluminium was extruded, although this was not tested on a real system. In the simulations, an initial linear temperature gradient was used on the billet. As part of the model predictive controller, state estimation was also implemented using the Extended Kalman Filter. The results showed that this method was able to give good estimates of the state of the system.

Bastani et al.[3] investigated strategies to achieve isothermal extrusion of aluminium using finite element simulations. The goal was to find out what effect several factors had on the exit temperature of the extruded aluminium. The factors they studied were the initial temperature at the front end of the billet, the initial axial temperature gradient, the cooling rate in the container and the ram speed. Their results showed that when the initial temperature gradient was low the exit temperature could be kept constant with a constant ram speed, while for higher initial gradients variable ram speed was needed. These two factors, initial temperature gradient and ram speed, were also found to be very important for keeping the exit temperature constant.

Bastani et al.[4] used model simulations to find operating conditions that would achieve isothermal extrusion while also minimizing radial variations in temperature and flow velocity in the billet during extrusion. Both 2D and 3D finite element models were used, and they showed that both these models yielded similar results. The factors studied were the ram speed, the initial temperature gradient of the billet and the cooling rate. The results showed that the initial temperature gradient of the billet had a significant effect on how much variation was observed in the exit temperature of the aluminium during extrusion. They also found that for low temperature gradients a constant ram speed could be used to keep the exit temperature constant, while for higher gradients a variable ram speed was necessary. These findings concur with the previous study by Bastani et al.[3].

Haseltine and Rawlings[7] studied different methods of state estimation. They compared the performance of the Extended Kalman Filter (EKF) and moving horizon estimation (MHE) on a nonlinear constrained system, and they found that MHE gave better state estimates and was more robust than the EKF. MHE did however have a higher computational load.

Rao et al.[12] investigated the use of MHE on constrained nonlinear discrete time systems. They concluded that the greatest practical advantage of MHE was the ability to incorporate constraints directly, which cannot be done when for example EKF is used. Computational load is however a problem in many applications. If MHE is to be used in practice, it needs to be able to estimate fast enough. They do however expect this problem to be solved in the near future as computers become more powerful and improved algorithms for computation are developed.

1.3 Scope of the project

This project aims to investigate if improvements of Hydro's current extrusion press operation procedures are possible through the use of open loop dynamic optimization. This is done by formulating and solving optimization problems aimed at achieving isothermal extrusion and high productivity. In addition, a parameter estimation procedure to fit a first principle model to the system will be developed. The goal is to evaluate the effectiveness of the moving horizon estimation method on the system, as well as determining which parameters should be estimated and what their initial values should be.

Part of the project was also to combine three separate models for system parts into a complete system model. The three original models were created by Cybernetica, and their development was not part of this project. The parameter estimation used a data series of measured data from 15 extrusion cycles performed by Hydro. No tests of the optimized press operation on the real system were possible to perform. The report will first describe the system considered, then present the model used to describe it. The optimization is then formulated, before the parameter estimation is explained. The results are then presented and discussed.

2 System Description

The system used in this project consisted of a heater for the aluminium billet, an extrusion press and the transport of the billet between these. This chapter provides an overview of each of these processes, both common practices in industry as well as the method used in the system this project is based on.

2.1 Heater

In the heater the billet is given a temperature profile intended to make the behaviour of the aluminium in the extrusion press better. The temperature at the point in the extrusion press where the aluminium gets its final shape is important for the product quality, and the temperature profile of the billet prior to extrusion can help keep it in the desired range. Common practice in industry is for the initial temperature profile of the billet, often called the taper, to be linear along the length of the billet, with the coolest end being extruded last. This way the reduction in temperature towards the back end of the billet is intended to compensate for the heat generation in the extrusion press. The taper is usually induced using a gas furnace or an induction heater, making accurate temperature control difficult [9].

Hydro makes use of an induction heater with four heating coils for a billet 0.9 m long, which is what was considered in this project. These coils are placed at 0.11 m, 0.34 m, 0.56 m and 0.79 m from the front end of the billet. An illustration is shown in Figure 2.1. The billet is first heated to approximately 460 °C in the front end and 410 °C in the back, and it is kept at this temperature for a while to reduce temperature gradients in the radial direction. This is called the saturation phase, and its length is determined by when there is space for the billet in the extrusion press. One press is often operated with several heaters, and there is therefore often some wait time in the heater. Before the billet is transferred to the press it is heated further. The temperature varies for aluminium alloys and product shapes, but for the considered product in the project the front end is heated to 530 °C and the back to 480 °C, which induces an axial temperature gradient in the billet.

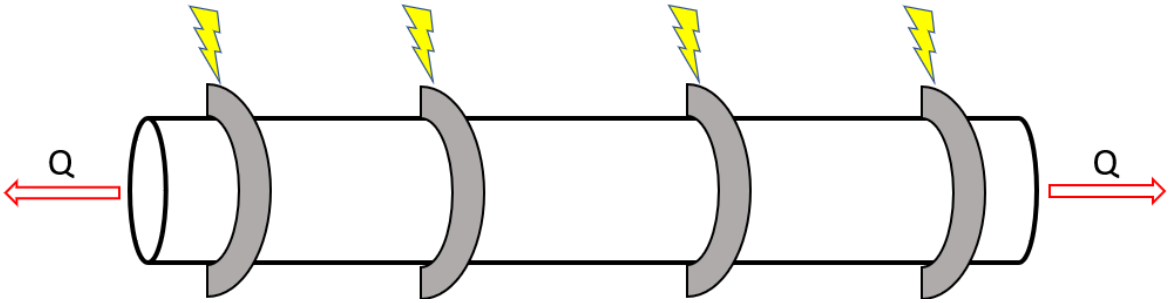

Figure 2.1: Illustration of the induction heater

2.2 Transit

In the transit phase, where the billet is being transported from the heater to the press, it is exposed to air at room temperature. Therefore, it loses heat to the environment and the temperature is reduced. Temperature gradients also shrink due to conductive heat transfer inside the billet. This is illustrated in Figure 2.2.

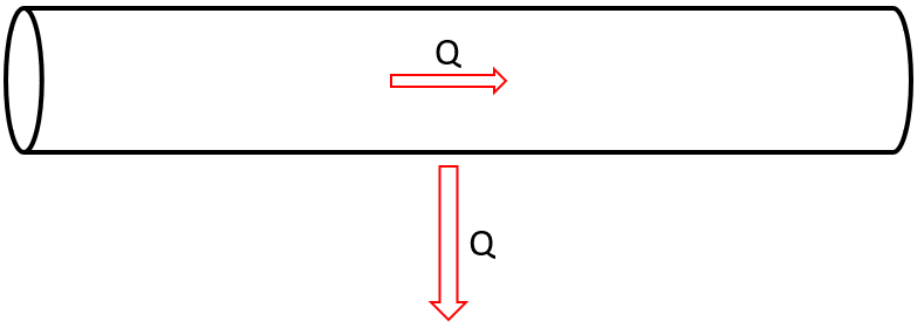

Figure 2.2: Illustration of the billet in transit

2.3 Extrusion press

Extrusion is a process shaping materials into straight profiles with a constant cross-sectional shape. This is done by pushing the material through a tool with a hole shaping it. This tool is called a die. Materials commonly treated using extrusion are metals, polymers and concrete. In this project, the material considered was aluminium. There are several methods of extrusion, and the two main ones are called direct and indirect extrusion. They differ in where the die is placed. In both methods the aluminium billet is placed in a container, and a hydraulic ram is used to apply pressure to it. In direct extrusion the die is placed on the opposite side of the container to the ram, as shown in Figure 2.3. In indirect extrusion however, a hollow ram is used. This means that the die is inside the ram, and the extruded material flows back through it. This is shown in Figure 2.4. The main practical differences this results in is that indirect extrusion has less heat generation from frictional forces, since the billet does not move relative to the container. In this project only direct extrusion will be considered, as this is the method used in the examined process.

Figure 2.3: Illustration of direct extrusion.

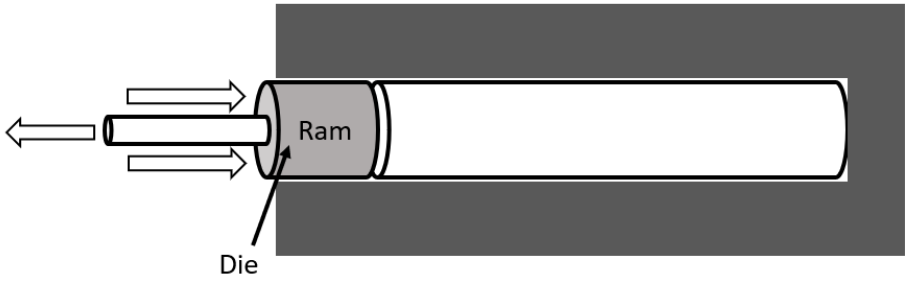

Figure 2.4: Illustration of indirect extrusion.

Extrusion is, along with rolling, one of the most common ways to shape aluminium. Achieving good product quality is however often complicated, especially when the extruded profiles are thin. The quality is highly dependent on the temperature during extrusion. If it is not within acceptable ranges deformation and tearing can occur. The most important temperature to control is located inside the die, where the final shaping of the aluminium happens. This is the highest temperature reached during extrusion, and it will be referred to as T_{peak}. The most common method in industry for regulating the temperature is to preheat the billet to create an initial taper. This counteracts the heat generation during extrusion, resulting in less variation in T_{peak}. The temperature is also dependent on the ram speed, and another possible way to control the temperature is therefore to vary the ram speed during extrusion [9]. Currently Hydro uses the method of inducing a temperature gradient on the billet, and operates with a fixed ram speed. To avoid material flow problems during extrusion, this gradient must be negative for the whole billet, meaning that the front end is warmest and the billet gets colder towards the back end.

2.3.1 Hydro Extruded Solutions - Precision Tubing

In this project one of Hydros extrusion processes is examined, and a more detailed description of it therefore follows. It is a process run by Hydro Extruded Solutions - Precision Tubing which produces thin walled, hollow profiles intended for use in heat exchangers. The product of interest in this project has a cross-sectional shape as shown in Figure 2.5. The walls are desired to be as thin as possible to reduce weight and increase heat transfer. Exact dimensions are confidential, but the thicknesses d are less than a millimeter and height and width are in the millimeter and centimeter range respectively.

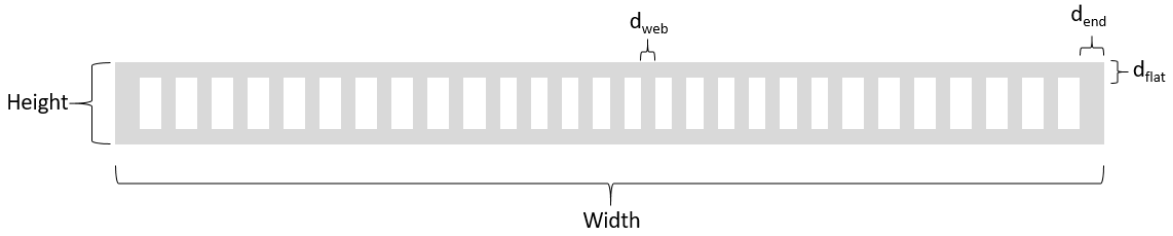

Figure 2.5: Illustration of the cross sectional shape of the extruded profile. d_{web} is the thickness of the inner webbing, and d_{end} and d_{flat} are the thicknesses of the end walls and the top and bottom walls respectively.

This product is produced in a multiport extrusion, which means there are several holes in the die used. An illustration of the die is shown in Figure 2.6. The light grey areas are where the aluminium passes through, and it is shaped further inside. The temperature T_{die} is an important measurement in the system, and T_{peak} is located where the final shape of the profile is achieved and it is the highest temperature the aluminium reaches during the process.

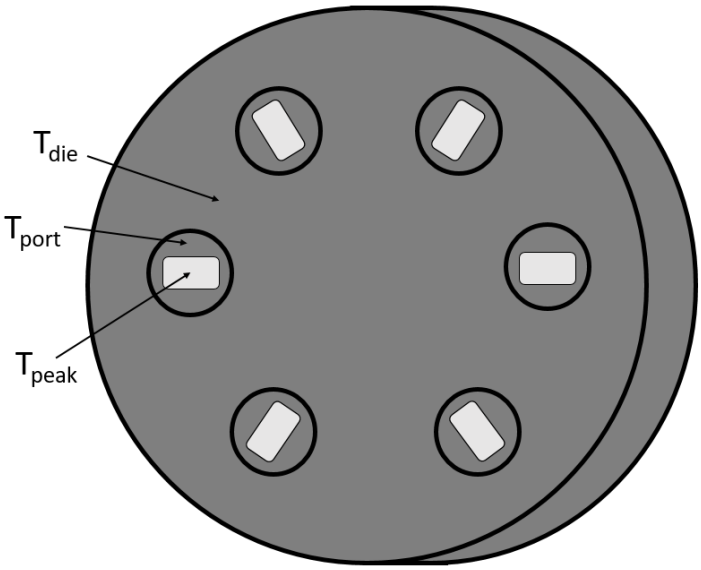

Figure 2.6: Illustration the die used in the extrusion. Aluminium passes through the light grey areas and gets the final shape inside the die. T_{die}, T_{port} and T_{peak} are important temperatures for the model. T_{peak} is located where the aluminium gets its final shape, further inside the die, while T_{die} and T_{port} are located on the surface.

3 Model Description

The model used in this project was made by combining three separate models developed by Cybernetica. Even though development of each model was not a part of this project, making a combined model of the whole system was. The complete model was then used in both the optimization and parameter estimation. A short description of the models for the heater, transit and extrusion press is therefore included, as well as how they were combined to a single model. As the models all have a similar structure, an introduction to their shared elements will be given first, before introducing the specific equations for each model.

All three models were formulated using a cylindrical coordinate system, because the aluminium billet is shaped like a cylinder. An illustration of this coordinate system can be seen in Figure 3.1, with the coordinates used included.

Figure 3.1: Illustration of the cylindrical coordinate system used in the models.

The models were then based on the equation of energy in cylindrical coordinates, shown in Equation 3.1.

$$\rho\hat{C}_p\left(\frac{\partial T}{\partial t}+v_r\frac{\partial T}{\partial r}+\frac{v_\theta}{r}\frac{\partial T}{\partial \theta}+v_x\frac{\partial T}{\partial x}\right)=-\left[\frac{1}{r}\frac{\partial}{\partial r}(rq_r)+\frac{1}{r}\frac{\partial q_\theta}{\partial \theta}+\frac{\partial q_x}{\partial x}\right] -\left(\frac{\partial \ln\rho}{\partial \ln T}\right)_p\frac{Dp}{Dt}-(\boldsymbol{\tau}:\boldsymbol{\nabla v}) \tag{3.1}$$

In this equation, T is the temperature of the aluminium, t describes time and x, r and θ are the coordinates shown in Figure 3.1. q_i and v_i with i = x, r, θ describe the conductive heat flux and velocity in the direction marked by the subscript. ρ and $\hat{C}_p$ are the density and heat capacity of the aluminium. The products of v_i and derivative of T on the left side of the equation describe convective heat transfer. The terms inside the square brackets on the right side describe the conductive heat transfer. $\frac{Dp}{Dt}$ is the substantial derivative of the pressure. The last term, $(\boldsymbol{\tau}:\boldsymbol{\nabla v})$, is viscous dissipation. It describes the degradation of mechanical energy in a material flow into thermal energy [5]. For all the models, axial symmetry was assumed. This means that all terms $\frac{\partial}{\partial\theta}(...)$ are equal to zero. According to Bastani et al. [4] this is a good approximation for this system. The conductive heat fluxes in the r- and x-direction were expressed as

$$q_r=-k_{\mathrm{Al}}\frac{\partial T}{\partial r} \tag{3.2}$$

$$q_x=-k_{\mathrm{Al}}\frac{\partial T}{\partial x} \tag{3.3}$$

using Fourier's law [8]. k_{Al} describes the thermal conductivity of the aluminium alloy used. Further simplifications and assumptions used on this equation for each individual model are described in Section 3.1, 3.2 and 3.3.

For all the models, the equation derived from Equation 3.1 is solved using finite differences [15]. The following approximations were therefore used:

$$\frac{\partial T}{\partial t}(i,j,k)\approx\frac{T(i,j,k+1)-T(i,j,k)}{\Delta t} \tag{3.4}$$

$$\frac{\partial T}{\partial r}(i,j,k)\approx\frac{T(i,j+1,k)-T(i,j-1,k)}{2\Delta r} \tag{3.5}$$

$$\frac{\partial T}{\partial x}(i,j,k)\approx\frac{T(i+1,j,k)-T(i,j,k)}{\Delta x} \tag{3.6}$$

$$\frac{\partial^2 T}{\partial r^2}(i,j,k)\approx\frac{T(i,j+1,k)-2T(i,j,k)+T(i,j-1,k)}{\Delta r^2} \tag{3.7}$$

$$\frac{\partial^2 T}{\partial x^2}(i,j,k)\approx\frac{T(i+1,j,k)-2T(i,j,k)+T(i-1,j,k)}{\Delta x^2} \tag{3.8}$$

In these equations the indexes i, j and k indicate the position in the x-direction, r-direction and time respectively. Δt, Δr and Δx are the distances between each point in time, the r-direction or the x-direction. Forward differences were used for first derivatives of T by t and x, while central differences were used for the rest. The billet was then discretized on the grid structure shown in Figure 3.2. It has 12 points in the x-direction and 6 in the r-direction.

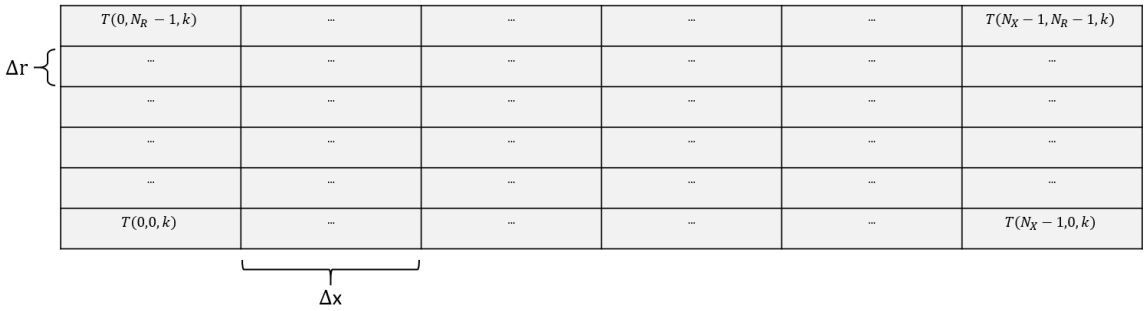

Figure 3.2: Illustration of the grid structure the billet is discretized on in the model. Δx and Δr are the distances between grid points in the axial and radial direction. N_X and N_R are number of points in each direction and are equal to 12 and 6 respectively.

3.1 Heater

In the model of the heater the following additional assumption were made:

- Aluminium is a solid in the temperature range $\Rightarrow v_i = 0$ for $i = x, r, \theta$ and $(\boldsymbol{\tau} : \boldsymbol{\nabla v}) = 0$
- ρ_{Al}, k_{Al} and $\hat{C}_p$ are constant in the temperature range
- Heat loss to the environment only at the front and back of the billet, and constant ambient temperature T_a
- Heat input from coils only at billet surface

Using these assumptions Equation 3.1 was simplified into

$$\begin{aligned} \frac{\partial T}{\partial t} &= \alpha_{\text{Al}} \left(\frac{1}{r} \frac{\partial}{\partial r} \left(r \frac{\partial T}{\partial r} \right) + \frac{\partial^2 T}{\partial x^2} \right) + \frac{Q}{\hat{C}_p \rho_{\text{Al}}} \\ -k_{\text{Al}} \frac{\partial T}{\partial x}\Big|_{\text{ends}} &= h(T_{\text{ends}} - T_a) \\ -k_{\text{Al}} \frac{\partial T}{\partial r}\Big|_{\text{surface}} &= 0 \\ -k_{\text{Al}} \frac{\partial T}{\partial r}\Big|_{\text{r=0}} &= 0 \end{aligned} \tag{3.9}$$

The first term on the right side of the equation for $\frac{\partial T}{\partial t}$ describes the internal heat conduction in the billet, both in the axial and radial direction. α_{Al} is the thermal diffusivity of the aluminium alloy, given by

$$\alpha_{\text{Al}} = \frac{k_{\text{Al}}}{\hat{C}_p \rho_{\text{Al}}}. \tag{3.10}$$

Q describes the heat input from the coils, and is only active at the surface underneath each coil. $h(T_{\text{ends}} - T_a)$ is the heat loss to the environment, which is only active at the front and back ends. h is the heat transfer coefficient between aluminium and air. The third line describes the assumption of only heat loss from the billet ends, while the fourth equation describes the assumption of axial symmetry.

3.2 Transit

The model of the transit of the billet from the heater to the extrusion press as based on the same assumptions as the heating model, but with two differences:

- There is no heat input Q
- There is heat loss from all of the billet surface, not just the front and back ends

This results in a similar model equation to the heater, but without the term for heat input:

$$\begin{aligned} \frac{\partial T}{\partial t} &= \alpha_{\mathrm{Al}} \left(\frac{1}{r} \frac{\partial}{\partial r} \left(r \frac{\partial T}{\partial r} \right) + \frac{\partial^2 T}{\partial x^2} \right) \\ -k_{\mathrm{Al}} \frac{\partial T}{\partial x}\Big|_{\mathrm{ends}} &= h(T_{\mathrm{ends}} - T_a) \\ -k_{\mathrm{Al}} \frac{\partial T}{\partial r}\Big|_{\mathrm{surface}} &= h(T_{\mathrm{surface}} - T_a) \\ -k_{\mathrm{Al}} \frac{\partial T}{\partial r}\Big|_{\mathrm{r=0}} &= 0 \end{aligned} \tag{3.11}$$

Here, the term $h(T_{\mathrm{ends}} - T_a)$ describes heat loss from the billet ends, while $h(T_{\mathrm{surface}} - T_a)$ is the heat loss from the rest of the surface. The last line of the equation describes the assumption of axial symmetry.

3.3 Extrusion press

For the model of the extrusion press, the following assumptions were used:

- ρ_{Al}, k_{Al} and $\hat{C}_p$ are constant in the temperature range
- Aluminium can be treated as a non-Newtonian incompressible fluid
- Material flow only in the axial direction $\Rightarrow v_r = v_\theta = 0$

Using these assumptions, Equation 3.1 can be simplified to:

$$\frac{\partial T}{\partial t} = \alpha \left(\frac{1}{r} \frac{\partial}{\partial r} \left(r \frac{\partial T}{\partial r} \right) + \frac{\partial^2 T}{\partial x^2} \right) - v_x \frac{\partial T}{\partial x} + \frac{\mu}{\rho_{\mathrm{Al}} \hat{C}_p} \left(\frac{\partial v_x}{\partial r} \right)^2 \tag{3.12}$$

Here, $v_x \frac{\partial T}{\partial x}$ is the convective term, which describes the heat transport due to material flow, while the last term on the right side of the equation is the simplified term for viscous dissipation. The viscosity μ is not constant, as the aluminium is assumed to be non-Newtonian. It is instead a function of the effective deviatoric stress and effective strain rate [2]. The model for the extrusion press also uses some additional control volumes to the ones shown in Figure 3.2. The grid structure with the additional control volumes is shown in Figure 3.3. The volumes named T_{feeder}, T_{port} and T_{peak} are places where the cross-sectional area of the billet is shrunk as it passes through the extrusion press and die, and the volumes named T_{exit} are parts of the billet which have already been extruded.
At each point where the cross-sectional area is reduced, a new flow velocity is calculated from the mass balance over the reduction zone and the assumption of incompressible fluid:

$$v_2 = \frac{A_1}{A_2} v_1 \tag{3.13}$$

The average flow velocity in the original billet grid is set equal to the ram speed. In these reduction regions a heat generation term is also added, but the equation used is classified and therefore cannot be disclosed in this report. The control volumes T_{Port} and T_{Peak} are very small compared to the

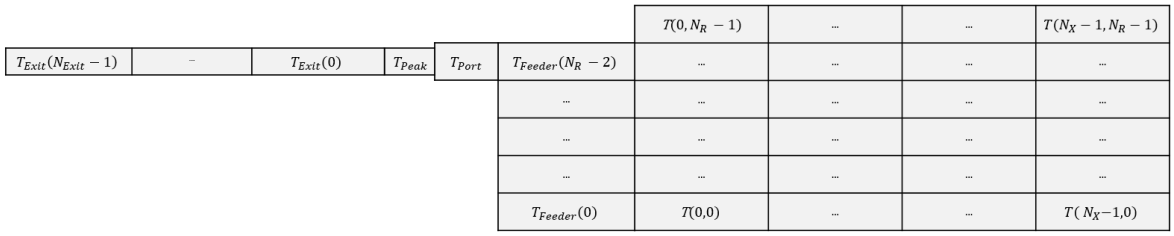

Figure 3.3: Illustration of the grid structure the billet is discretized on in the extrusion model.

others, and a quasi steady state assumption was therefore made to calculate the states here. This is a common way to avoid numerical problems caused by stiff systems [17], and it assumes that since parts of the system changes much faster than others they can be assumed to change "instantaneously" compared to slower parts of the system, and thus always be at steady state. Their values can therefore be directly calculated from the values in neighbouring control volumes.

3.4 Combined model

Equation 3.9, 3.11 and 3.12 together form the model for the whole extrusion process. The model also contains parts not disclosed in this report, as these equations are confidential. Therefore, several of the parameters estimated later in the report can not be found in the presented model equations. They are nevertheless important for model behaviour. Rigid specification of time in each equation was necessary to be able to use the model for optimization, since the time periods where the different variables were active had to be specified before the simulation started. When the process starts, the equation for the heater is used. The heating coils are allowed to be active in a specified time period, between $t = 30\,\text{s}$ and $t = 60\,\text{s}$ after which the model switches to the equation for transit. This equation is used for a specified amount of time, 93 s, approximately the time for the billet to be transferred from the heater to the press in the real system. Then the model switches to the equation for the extrusion press, which is used until the ram reaches its end position, which means the extrusion is finished. After this, all state derivatives are set to zero.

When the model was used for parameter estimation this specification of time was not necessary. Instead, logic based on the logged data was used to determine when each equation should be used. The model was switched from the heater equation to transit when all heating coils and temperature measurements in the heater were turned off. It was then switched from transit to the extrusion press model when a signal for billet change in the press became active. It was then set to finished when the billet length had reached its minimum value. A variable for the billet phase was used to keep track of which equation to use. When the billet phase is 0 the billet is in the heater, when it is 1 it is in transit and when it is 2 it is in the press. When the extrusion is finished and the heater is waiting for a new billet the billet phase is equal to 3. An overview of the billet phase values and corresponding models can be found in Table 3.1. Figure 3.4 shows T_{peak}, ram speed and billet length for a simulation of three full extrusion cycles. T_{peak} is only calculated when the billet is in the press, which is the reason the value is only shown for some of the simulation time. In the plot of the ram speed, the peaks before and after extrusion correspond to the ram moving into position before and after the extrusion is performed. They therefore do not represent billet movement. Figure 3.5 shows billet surface temperatures, heating coil status and billet phase. The plot of the billet surface temperature is zoomed in around the region the temperature lies in for most of the process to better illustrate its behaviour. This means the start of each heating cycle, where it is heated from 20 °C to 400 °C, is not shown. Predicted values for measurements made during these extrusion cycles can be found in Section 6.3.1. They show some difference between measured and predicted values, but the model generally managed to capture the behaviour of the system well.

Table 3.1: Billet phase values and corresponding models.

Billet phase	Model used
0	Heater
1	Transit
2	Extrusion press
3	Idle

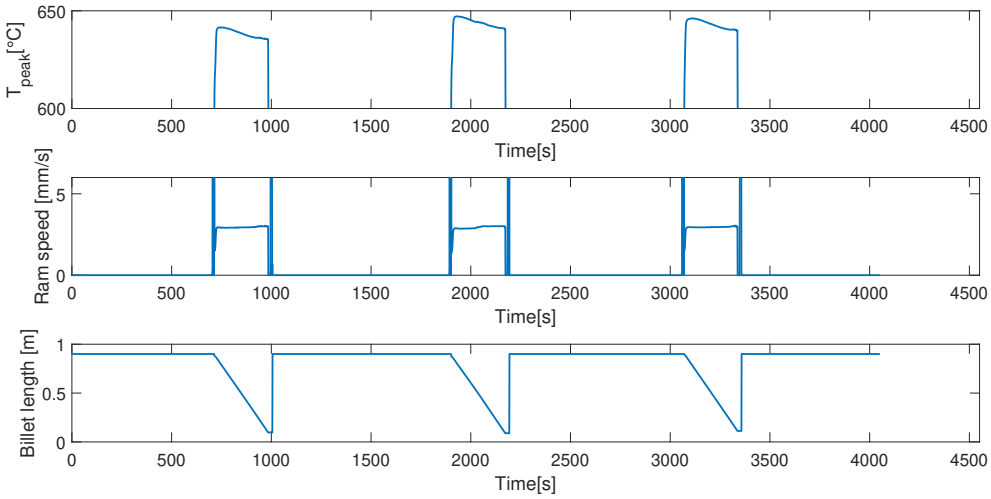

Figure 3.4: T_{peak}, ram speed and billet length from a simulation using logged data from Hydro.

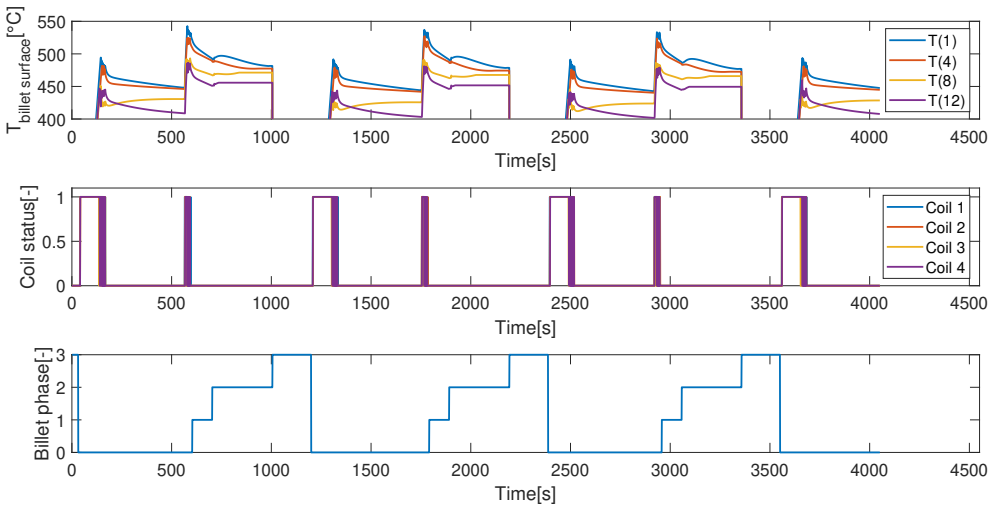

Figure 3.5: Billet surface temperatures, heating coil status and billet phase from a simulation using logged data from Hydro.

3.5 Software

A description of the software used in the project, both for model implementation, optimization and parameter estimation, is given below. All software used was developed by Cybernetica [14].

- **Cybernetica Model and Application Component:** A template for model implementation as well as optimization problem and parameter estimation formulation in the programming language C.
- **Cybernetica CENIT:** Software used for optimization and parameter estimation. Consist of two parts, the CENIT Kernel and CENIT MMI. The Kernel does the computation, while MMI is the user interface. This software was used only for optimization in this project.
- **Cybernetica RealSim:** Software for model simulation. Used to test the optimizations from CENIT by mimicking the real system.
- **Cybernetica Modelfit:** Software used for parameter estimation.

4 Dynamic Optimization

In optimization problems the aim is to minimize or maximize the value of a scalar function called the cost or objective function by adjusting the values of certain variables in the function. The objective function is commonly represented by the symbol f. The variables are often called inputs or MV's, which stands for manipulated variables, and the are usually represented by the letter u. The variables are often subject to constraints on their values, either equalities or inequalities. They are usually given the symbols c and g respectively [10]. The optimization problem can then be formulated as

$$\begin{aligned} &\min_{u} \ f(u) \\ &\text{s.t. } g(u) \leq 0 \\ &\quad\ \ c(u) = 0. \end{aligned} \tag{4.1}$$

To gain a better understanding of optimization, a simple example can be formulated. Given the objective function $f(u) = u_1^2 + u_2^2$ and the constraint $g(u) = (u_1 - 3)^2 - 2u_2 \leq 0$ the optimization problem can be written as

$$\begin{aligned} &\min_{u_1, u_2} \ u_1^2 + u_2^2 \\ &\text{s.t. } (u_1 - 3)^2 - 2u_2 \leq 0 \end{aligned} \tag{4.2}$$

An illustration of this problem is shown in Figure 4.1. Here, the feasible region, where the constraints are satisfied, is above the line $c(u)$. The contour plot of $f(u)$ shows lines where the objective function has constant value. The solution is the point in the feasible region which is closest to the unconstrained optimum of $f(u)$, which is $u = [0, 0]$. For this problem this value is approximately $u = [1.54, 1.06]$.

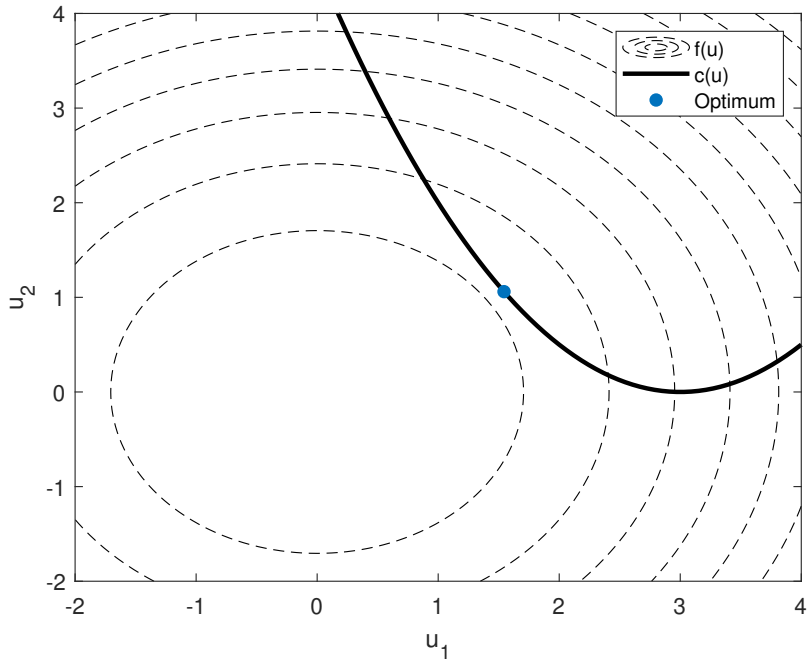

Figure 4.1: Illustration of the optimization problem formulated in Equation 4.2.

In dynamic optimization a dynamic model is included as an equality constraint in the optimization problem[6]. The goal is then to calculate the optimal behaviour of the system described by this model. What characterizes optimal behaviour is defined by the objective function, and it commonly includes parts to keep certain values close to set points, minimize energy usage or maximize production. For discrete time models the optimization problem can be formulated as

$$\begin{aligned} \min_u \ & \sum_{t=0}^{N-1} J(x_{t+1}, u_t) \\ \text{s.t. } & x_{t+1} = g(x_t, u_t) \\ & c(x_t, u_t) \leq 0 \\ & x_{min} \leq x_t \leq x_{max} \\ & u_{min} \leq u_t \leq u_{max} \\ & -\Delta u_{max} \leq \Delta u_t \leq \Delta u_{max} \\ & x_0, u_{-1} = \text{given} \end{aligned} \tag{4.3}$$

Here, $J(x_{t+1}, u_t)$ is the part of the objective function at each point in time t, and the sum of all $J(x_{t+1}, u_t)$ in the prediction horizon N is the total objective function. The vector x_t contains the states of the system at time t, and the discrete time dynamic model is the equality $x_{t+1} = g(x_t, u_t)$. $c(x_t, u_t)$ contains path constraints for the process, while (x_{min}, x_{max}) and (u_{min}, u_{max}) describe lower and upper limits for states and inputs respectively. This can for example be $(0, 1)$ for the position of a valve, which has to be between fully closed (0) and fully open (1). Inputs also often have limits on how much they can change for each step in time. The change is calculated as

$$\Delta u_t = u_t - u_{t-1} \tag{4.4}$$

and limited by the value of Δu_{max}. The initial condition of the system, x_0 and u_{-1}, is also required as a starting point for the optimization.

This project considered dynamic optimization of a process for aluminium extrusion. In the first part the goal was to keep the temperature T_{peak} close to a set point, and the objective function therefore only contained a set point tracking term. Here, only the ram speed was used as an input, while logged data from the actual system was used for the heating of the billet. This is described in Section 4.2. In the second part the additional goal of performing the extrusion as fast as possible was added. The objective function therefore also contained a term for maximizing the ram speed, and the set points for the temperature by the coils in the heater were added as inputs in the optimization problem. This is described in Section 4.3.

4.1 Constraints

Both of the inputs in the optimization problem are subject to constraints, to ensure that they have values that are physically feasible. The lower limits for the temperature set points in the heater were set to 0 °C, and the upper limits were set to the melting point of aluminium, equal to 660 °C[11]. For the ram speed, the lower limit was set to 0 mm/s, as the ram is not allowed to move backwards, and the upper limit was set to 5 mm/s. The exact value for the highest speed the ram is capable of is uncertain, and the value of the upper limit was therefore set to be significantly higher than the usual operating speed of 3 mm/s. The acceleration of the ram was also limited to 0.4 mm/s^2, although the exact value for the extrusion press is uncertain here too.

4.2 Optimizing ram speed

The optimization problem with only the ram speed as an input is shown in Equation 4.5. The objective function contains one part which punishes deviation in T_{peak} from its set point, which is the set point tracking, and one which punishes breaking the inequality constraint on T_{peak}. This is called a soft constraint, since the value of ϵ_t adapts to ensure that it is always fulfilled, but nonzero values for ϵ_t induces a heavy penalty in the objective function and is therefore avoided by the optimization where possible. The reason for this formulation is to ensure that the problem will still converge to a solution even if T_{peak} sometimes is far from the optimum, like for example close to the start of the extrusion where the value is 520 °C. This low initial condition is also the reason that the objective function starts at $t = 380\,\text{s}$, while the extrusion itself starts at $t = 370\,\text{s}$. The first seconds there will always be significant deviation from the set point, no matter what the input does, and these time steps therefore serve no purpose in the optimization problem. It can be seen that the extrusion itself starts at different times in this optimization problem and the one with optimization of both ram speed and heating shown in Section 4.3. This is because only the end of the heating cycle was simulated in this optimization, since this would reduce the prediction horizon and thus also the computational cost of solving the problem without reducing accuracy as logged data was used to simulate the heating.

The input, u_{RamSpeed}, was allowed to be changed every second for the first 15 s after the extrusion started, after which it was allowed to adjust the speed every 10 s. Between these points a first order hold was used, which means the value of the input varied linearly between each point

$$
\begin{aligned}
\min_{u_{\text{RamSpeed,t}}} \quad & \sum_{t=380}^{N-1} (T_{\text{peak, t+1}} - T_{\text{peak, sp}})^2 + \rho\epsilon_{t+1} \\
\text{s.t. } & x_{t+1} = g(x_t, u_{\text{RamSpeed, t}}) \\
& c(x_t, u_{\text{RamSpeed, t}}) \leq 0 \\
& x_{min} \leq x_t \leq x_{max} \\
& T_{\text{peak, sp}} - 5\,^\circ\text{C} - \epsilon_t \leq T_{\text{peak, t}} \leq T_{\text{peak, sp}} + 2\,^\circ\text{C} + \epsilon_t \\
& \epsilon_t \geq 0 \\
& 0\,\text{mm/s} \leq u_{\text{RamSpeed, t}} \leq 5\,\text{mm/s} \\
& \Delta u_{\text{RamSpeed, t}} \leq 0.4\,\text{mm/s}^2 \\
& T_{\text{peak, 370}} = 520\,^\circ\text{C} \\
& u_{\text{RamSpeed, 369}} = 0\,\text{mm/s}
\end{aligned}
\tag{4.5}
$$

4.3 Optimizing ram speed and heating

The optimization problem with both the initial heating and ram speed as inputs is shown in Equation 4.6. The input vector u_{T} contains the optimal surface temperatures underneath the heating coils, where the temperature is measured. For a billet of length 0.9 m this means it has four temperatures to optimize. As can be seen from the simulation in Figure 3.5 the heating has three distinct phases. First it is heated to approximately 40 °C below its final temperature, and then the heating coils are turned off for approximately 390 s. This is called the saturation phase, and helps to reduce radial temperature gradients in the billet. The time spent in this phase is determined by the extrusion press. When it is done with the previous billet the one currently in saturation can start its final heating to the desired temperature. As can be seen from the simulation the heating coils are turned on and off for a period after the billet reaches the final temperature. This is to keep the billet temperature at the desired level while also adding more energy, which reduces the temperature loss during the transit to the extrusion press. Data from Hydro showed that this final heating phase took approximately 30 s. To ensure that the optimization results from this project are physically feasible on the real system, this behaviour was included in the optimization. The time the billet spends in different phases was

therefore included in the model. These time periods are shown in Table 4.1. Specifying the time the billet spends in each phase was necessary to determine at which time steps the optimization could use the different inputs. The ram speed could for example only be used in the extrusion phase. In the real system these time periods are expected to vary some, but the specified time table is expected to be a good approximation of the average behaviour of the billets.

Table 4.1: Time steps where the billet enters a new phase.

Billet phase	Time [s]
First heating	30
Saturation	160
Final heating	550
Transit	580
Extrusion	673

The objective function now contains a part to maximize the ram speed as well as the parts explained in Section 4.2. The scalar variables q_1 and q_2 are used to prioritize between the parts of the objective function. A new constraint on the axial temperature gradient of the billet during the final heating period was also added. To avoid problems with material flow due to the temperature's effect on viscosity, as described in Section 2.3, the axial temperature gradient must be negative, so that the billet is colder towards the back end. This is ensured with the new constraint. Logic to control the heating coils themselves was also included in the model for this optimization problem, as logged data could no longer be used. While the billet was in the first of final heating phase, the coils were left on as long as the temperature on the billet surface beneath the coils was below the corresponding optimal temperature in u_T.

$$
\begin{aligned}
\min_{u_{\mathrm{T}}, u_{\mathrm{RamSpeed,t}}} \quad & \sum_{t=683}^{N-1} q_1 (T_{\text{peak, t+1}} - T_{\text{peak, sp}})^2 + \rho \epsilon_{t+1} + \sum_{t=673}^{N-1} q_2 (u_{\text{RamSpeed, max}} - u_{\text{RamSpeed, t}})^2 \\
\text{s.t.} \quad & x_{t+1} = g(x_t, u_{\mathrm{T}}, u_{\text{RamSpeed, t}}) \\
& c(x_t, u_{\mathrm{T}}, u_{\text{RamSpeed, t}}) \leq 0 \\
& x_{min} \leq x_t \leq x_{max} \\
& T_{\text{peak, sp}} - 5\,^{\circ}\mathrm{C} - \epsilon_t \leq T_{\text{peak, t}} \leq T_{\text{peak, sp}} + 2\,^{\circ}\mathrm{C} + \epsilon_t \\
& \epsilon_t \geq 0 \\
& 0\,^{\circ}\mathrm{C} \leq u_{\mathrm{T}} \leq 660\,^{\circ}\mathrm{C} \\
& \left(\frac{dT_{\text{billet}}}{dx} \right)_{\text{t}\in[550,\ 580]} \leq 0 \\
& 0\,\mathrm{mm/s} \leq u_{\text{RamSpeed, t}} \leq 5\,\mathrm{mm/s} \\
& \Delta u_{\text{RamSpeed, t}} \leq 0.4\,\mathrm{mm/s}^2 \\
& T_{\text{peak, 673}} = 520\,^{\circ}\mathrm{C} \\
& u_{\text{RamSpeed, 672}} = 0\,\mathrm{mm/s}
\end{aligned}
\tag{4.6}
$$

5 Parameter Estimation

In industrial processes the amounts of available measurements are usually limited, and the parameters and states that are important in the process model are often not measurable. The measurements that can be made are also subject to noise. For example, concentration measurements are often not available, as these are more costly to perform than pressure or temperature measurements. Parameters like reaction rates and heat transfer coefficients are also not possible to measure directly. This means the accuracy of the model is reduced, especially for non-stationary processes where the values of states and parameters vary during the process. If the model is used in optimization, bad parameter estimates will make the optimal behaviour for the model sub optimal for the real system. Accurate parameter estimation is therefore crucial for optimizing processes. To achieve good estimates of the model parameters, they need to be estimated based on the available measurements, which are compared to predicted values from the model. Parameter values are then adjusted to make the difference between them small. Two common methods of estimation are Kalman filter and moving horizon estimation (MHE).

For linear and unconstrained systems where noise is normally distributed, the Kalman filter is established as the optimal estimator [7]. It is a recursive approach based on estimating the covariance between measurements and predicted values, and using a combination of these values to determine how much parameter values should be adjusted. For non-linear models the Kalman filter cannot be used directly, since it assumes a linear system. The most common solution is to use the Extended Kalman filter (EKF) instead. It works by linearizing the model in the current time step, and then using the common Kalman filter on the linearized model. For models with a high degree of non-linearity this method can yield inaccurate results, as the linearized model captures the behaviour of the original model poorly. Constraints in the parameters can also be difficult to incorporate [7]. This is not a problem for MHE, which can use non-linear models directly in estimation. It works by solving an optimization problem minimizing the difference between past measured and predicted values by adjusting the parameters, and is therefore well suited for handling both constraints and non-linear models. On-line implementation of MHE has however been limited by the computational cost associated with solving the optimization problem [12]. This limitation is not as relevant for batch processes, like aluminium extrusion, as the parameter estimation can be performed between batches. MHE was therefore investigated as a method for parameter estimation in aluminium extrusion in this project, and a detailed explanation of the method can be found in Section 5.1.

5.1 Moving Horizon Estimation

Moving horizon estimation is a method of parameter estimation which uses a sliding window of measured and predicted values in the system to formulate an optimization problem to find the best parameter values. At each step in time a new measurement is added to the data set and the oldest one is removed, and the optimization is then performed with the updated data. An illustration of this procedure is shown in Figure 5.1.

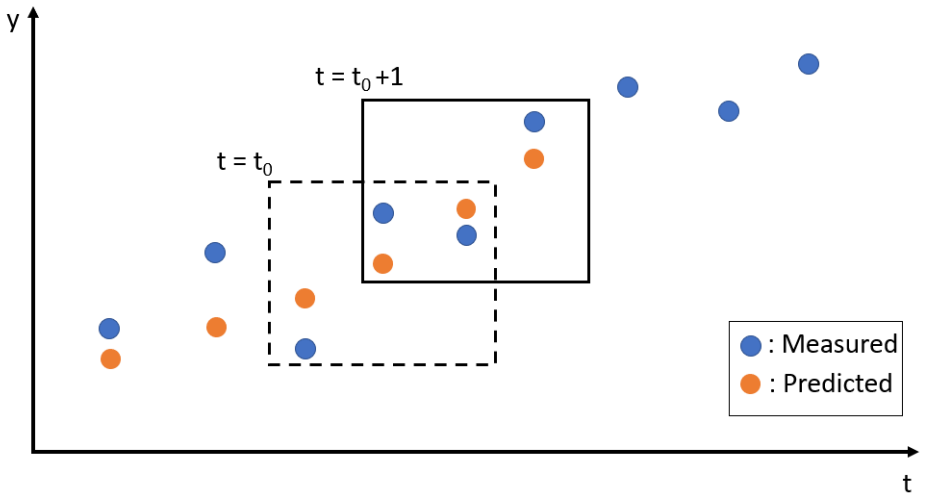

Figure 5.1: Illustration of the MHE procedure for updating the data set.

This updating of the data set is the origin of the name "moving horizon". The optimization problem can be formulated as [13]

$$\begin{aligned} J_N = \min_{\theta_0,\ldots,\theta_N} \; & J_0(\theta_0) + \sum_{i=0}^{N-1} \nu_i^T V_i^{-1} \nu_i + \sum_{i=1}^{N} \omega_i^T W_i^{-1} \omega_i \\ \text{s. t.} \quad & x_{i+1} = g(x_i, \theta_i, \nu_i) \\ & y_i = h(x_i, \theta_i) + \omega_i \\ & x_0 = \text{given} \end{aligned} \tag{5.1}$$

The objective function J_N consists of three parts. $\sum_{i=1}^{N} \omega_i^T W_i^{-1} \omega_i$ aims to minimize the difference between predictions and measurements in the estimation horizon, while $\sum_{i=0}^{N-1} \nu_i^T V_i^{-1} \nu_i$ aims to reduce how much the estimator varies the parameters. Here, V_i and W_i are covariance matrices for process and measurement noise, ν_i and ω_i. ω_i therefore describes the difference between measured and predicted values. N is the number of data points in the estimation horizon and θ_i is the vector containing the parameters. $J_0(\theta_0)$ is an approximation of the arrival cost, which summarizes past information earlier than the estimation horizon [1]. Here, a smoothing scheme is used to for the approximation. It is based on the conditional density of the smoothed parameter estimate for data before the estimation horizon, but the actual equations used here are confidential and cannot be disclosed in this report. x_i is the states of the system and $g(x_i, \theta_i)$ describes the system model, which can be non-linear. $h(x_i, \theta_i)$ is the function to calculate the outputs y_i from the model. The MHE is tuned by adjusting values in the diagonals of the covariance matrices V_i and W_i, as well as weights for each parameter in the arrival cost. A high arrival cost weight means the algorithm trusts the initial parameter values more, which reduces how much the parameter value is adjusted by the estimator. The values in W_i determine how much the estimator weights prediction errors for the different measurements, while the values in V_i affect how much it punishes variations in the different parameters.

5.2 Measurements and Parameters

Several measurements were available for use in parameter estimation. In the heater, one temperature sensor was placed in each of the induction coils, resulting in 4 measurements of surface temperature underneath the coils illustrated in Figure 2.1. In addition, the temperature was measured at the front and back end of the billet. Several parameters were available for estimation in the heater:

- $h_{\text{front}}[\text{W/m}^2\text{K}]$: Heat transfer coefficient between front end of the billet and air.
- $h_{\text{back}}[\text{W/m}^2\text{K}]$: Heat transfer coefficient between back end of the billet and air.
- BiasCoil(i)[K/s], i = 1, 2, 3, 4: The offset from expected added energy for each induction coil in the heater, formulated as an offset from the expected temperature change the added energy would induce.
- $CF_{\text{k,Al}}[-]$: Correction factor for the conductivity of aluminium.

In the transit phase the billet passes through a measuring station where the surface temperature is measured at 4 points for billets of the size investigated in this project. Here, one measurement is made at each point per billet. This is used to estimate the value of the heat transfer coefficient between the billet surface and air, $h_{\text{billet}}[\text{W/m}^2\text{K}]$.

In the extrusion press, two measurements are made. A thermocouple measures the temperature inside the die T_{die}, which means it shows the temperature of the die itself and not the aluminium. An IR-sensor also measures the temperature of the aluminium after it has been extruded, T_{exit}. The location of T_{die} is shown in Figure 2.6. The IR-sensor for T_{exit} is located 2.5 m after the aluminium exits the press. The parameters to be estimated are:

- $CF_{\text{viscous dissipation}}[-]$: Correction factor for the viscous dissipation term in Equation 3.12.
- $CF_{\text{reduction regions}}[-]$: Correction factor for heat generation in the reduction regions.
- $h_{\text{AlAir}}[\text{W/m}^2\text{K}]$: Heat transfer coefficient between the extruded aluminium and air.
- $\tau_{\text{die}}[\text{s}]$: Time constant for a heat loss term from the die to its surroundings, which could not be included in the model description.
- $h_{\text{AlSteel}}[\text{W/m}^2\text{K}]$: Heat transfer coefficient between aluminium and steel.

6 Results and Discussion

In this section the results from the project will be presented and discussed. First, the solutions to the optimization problems described in Equation 4.5 and 4.6 using the original model parameter values will be presented. Then, the results from the parameter estimation will be shown, before the optimization results with updated model parameters are presented and compared to the ones with original parameters. The two main considerations when comparing optimization results are the deviation in T_{peak} from its set point and how fast the extrusion is performed. To show improvements made by the optimization the results are compared to data from an extrusion performed by Hydro using current operating procedures. A plot of T_{peak} and the ram speed is shown in Figure 6.1. The high peaks in ram speed at the start and end of the extrusion come from moving the ram into position before and after the extrusion, and thus does not represent the movement of the billet itself. The extrusion is commonly performed with a constant ram speed of 3 mm/s, which before parameter estimation gives a peak temperature starting at approximately 640 °C, which falls to around 635 °C during extrusion. The extrusion time, not including heating and transit, is typically around 300 s.

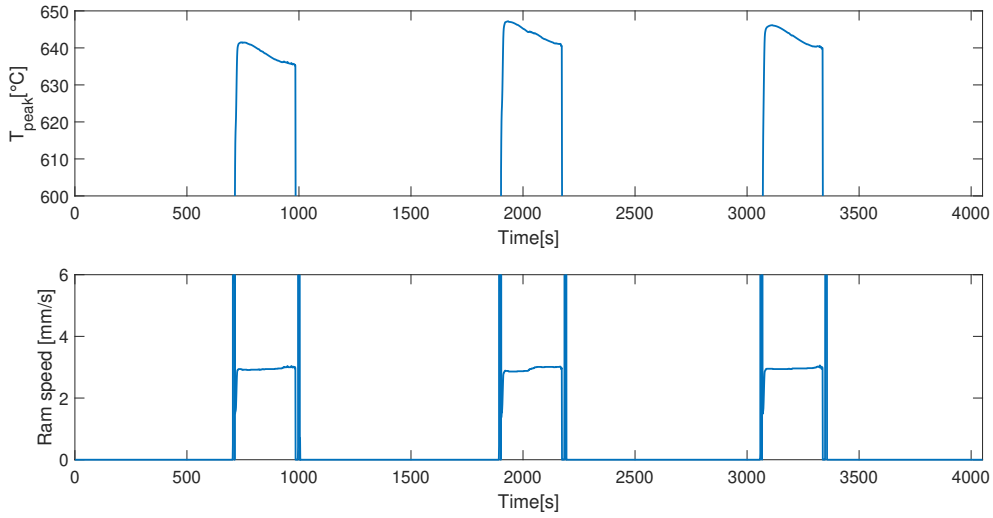

Figure 6.1: T_{peak} and the ram speed from a simulation with original parameter values and no MHE.

6.1 Optimizing Ram Speed using Original Parameters

This section describes the results from solving the optimization problem posed in Section 4.2. Here, data from Hydro was used to simulate the initial heating of the billet and only the ram speed was optimized. This allows one to see what process improvements can be achieved without optimizing the heating process. The value used for the set point of T_{peak} was 620 °C. Figure 6.2 shows the results from the optimization of the ram speed using the original parameter values. The temperature set points in the heater are shown in Figure 6.3, and exact values can be found in Table 6.3. As only the ram speed was optimized here, these set points are estimated from measurements in the logged data from Hydro used to simulate the heater in this optimization. This use of logged data is intended to ensure realistic billet temperatures, and it is the reason the extrusion itself doesn't start before $t = 370$ s. Hydro currently operate with linear initial temperature gradients, and the small deviation from linearity observed in Figure 6.3 was most likely due measurement noise. Figures showing the billet temperature during the process and heating coil activity are shown in Section A.1. The results show very good set point tracking for T_{peak}, but the ram speed was lower than in the logged data

shown in Figure 6.1. This resulted in an extrusion time, not including heating and transit, of 538 s. The low ram speed was caused by the low set point for T_{peak} compared to its values when using logged data for the ram speed. This indicates that either the set point used for T_{peak} was too low, or the heat generation in the model was too high. The heat generation will be investigated further in the parameter estimation.

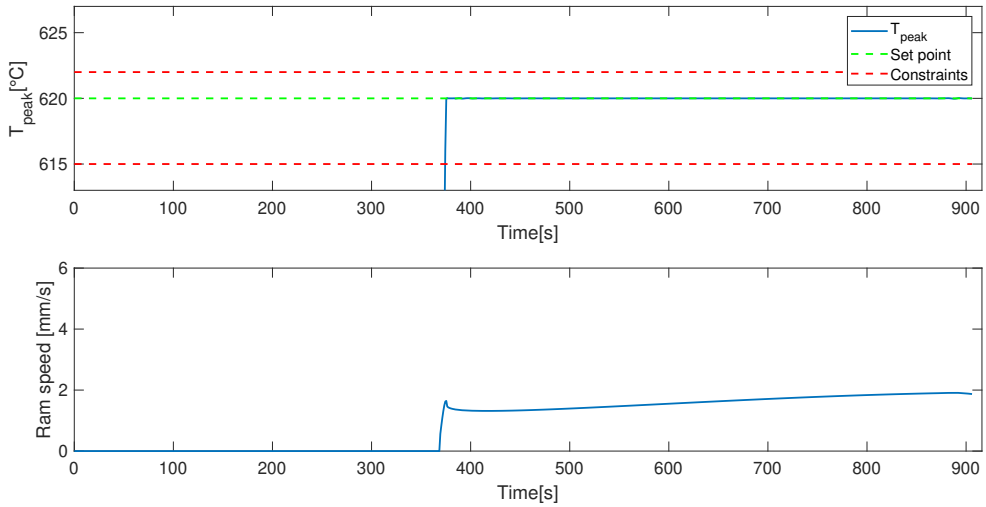

Figure 6.2: Optimized ram speed and T_{peak} with original parameter values.

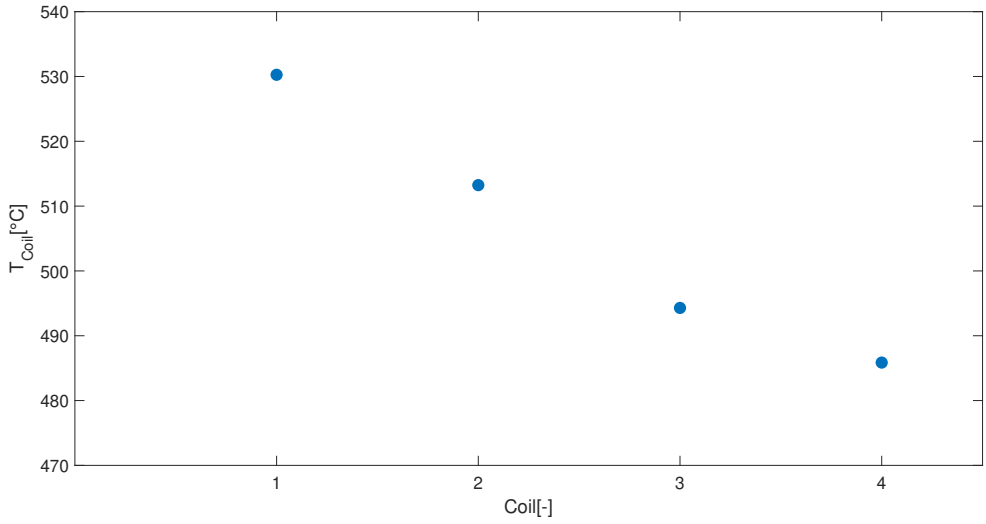

Figure 6.3: Temperature set points in the heater from logged data from Hydro.

6.2 Optimizing Ram Speed and Heating using Original Parameters

This section describes the results from solving the optimization problem formulated in Section 4.3. Here, both the ram speed and the temperature set points in the heater were used as manipulated variables and the original parameter values were used in the model. The resulting values from T_{peak} and ram speed are shown in Figure 6.4, and the values for the temperature set points are shown in Figure 6.5. The exact temperature values are also shown in Table 6.3. Figures showing the billet temperature during the process and heating coil activity are shown in Section A.3. In the objective function of the optimization problem, the value 20 was used for q_1 and 10 for q_2. The results show very good set point tracking for T_{peak} and the extrusion time, not including heating and transit, was 229 s. The new extrusion time was therefore less than half of the one where only the ram speed was optimized. This was a significant reduction made possible by lowering the temperature set points in the heater. The set points from the logged data were between 530 °C and 485 °C, and the new ones approximately between 470 °C and 390 °C. Much higher ram speed was therefore required to reach the set point for T_{peak}. It can also be seen that the temperature gradient was not quite linear. The temperature difference between the coils increased slightly towards the back end of the billet, with a difference of 23 °C between coil 1 and 2, 24 °C between coil 2 and 3 and 32 °C between coil 3 and 4. This might explain how the ram speed could keep increasing towards the end of the extrusion cycle. As the temperature gradient of the incoming part of the billet kept increasing towards the end of the cycle, higher and higher ram speed was required to compensate.

The formulation of the optimization in the heater proved to give an unstable solution to the problem. As described in Section 4.3 the heating coils were left on as long as measured temperature by the coils was below the optimized set point for each coil. As the model used a sampling time of 1 s, this meant that for the part when the temperature had reached the set point but the transit period had not started yet the coils were left on for a full second each time the temperatures fell below the set points again. This resulted in quite large and unpredictable temperature variations towards the end of the heating period, which made it difficult for the optimization problem solver to linearize the problem, as small changes in the values of the set points gave unpredictable changes in the measured coil temperature at the end of the heating cycle. To increase the stability of the optimization problem logic was therefore implemented to make the measured temperatures more stable towards the end of the heating period. The last 10 s the power of each coil was reduced, so that they could add enough energy to keep the temperature at the set point without high peaks every time the coil turned on. This would not be realizable on the real system, as the coil power is fixed, and was just added to make the solver more well behaved. The behaviour could however be mimicked in the real system by having the coils turned on for shorter periods than 1 s.

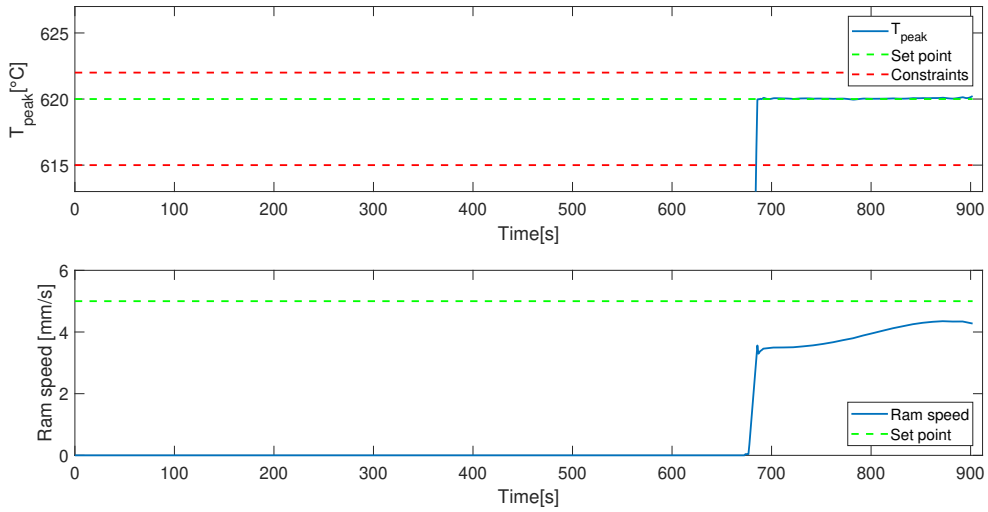

Figure 6.4: Optimized ram speed and T_{peak} with original parameter values from optimization of both ram speed and heating.

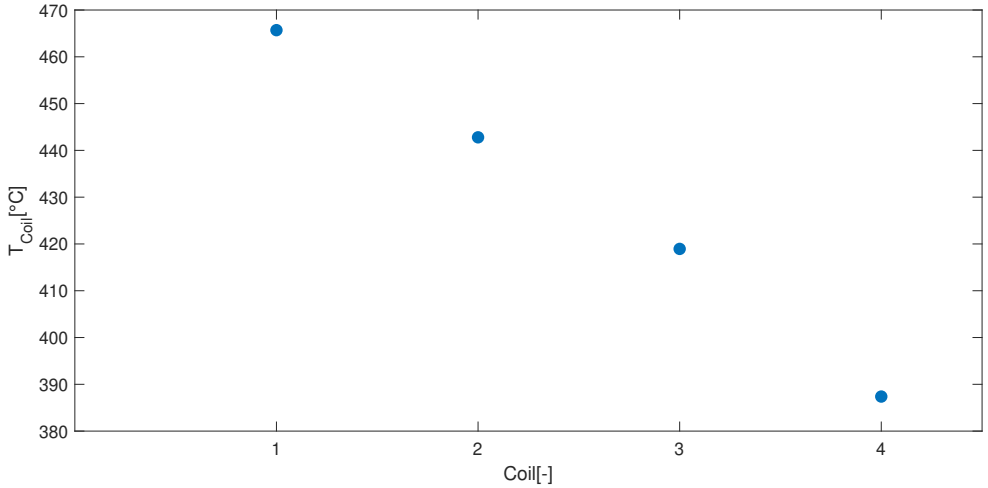

Figure 6.5: Optimized temperature set points in the heater for optimization using original parameter values.

6.3 Parameter Estimation

In this section the results from the parameter estimation using moving horizon estimation (MHE) are presented. The goal was to find out which parameters should be estimated and which should be kept constant, as well as finding good initial guesses for the values of estimated parameters. Before investigating this, the MHE was tuned to give stable parameter estimates. These tunings are shown in Table 6.1.

Table 6.1: Tuning parameters used for MHE. W, V and arrival cost are described in Section 5.1. W_j and V_j describe the values along the diagonal of each matrix corresponding to the measurement or parameter in the column "Variable".

Variable	Type	W_j	V_j	Arrival cost weight
T_{front}	Measurement	1	-	-
T_{back}	Measurement	1	-	-
$T_{\text{coil i}}$, i = 1,2,3,4	Measurement	1	-	-
h_{front}	Parameter	-	0.1	0.1
h_{back}	Parameter	-	0.1	0.1
$CF_{\text{k,Al}}$	Parameter	-	0.0001	0.0001
BiasCoil_i, i = 1,2,3,4	Parameter	-	0.0001	0.01
$T_{\text{meas. station i}}$, i = 1,2,3,4	Measurement	0.1	-	-
h_{billet}	Parameter	-	0.1	0.8
T_{die}	Measurement	0.2	-	-
T_{exit}	Measurement	1	-	-
$CF_{\text{viscous dissipation}}$	Parameter	-	0.0001	0.0008
$CF_{\text{reduction regions}}$	Parameter	-	0.0001	0.0008
h_{AlAir}	Parameter	-	0.003	0.008
h_{AlSteel}	Parameter	-	2	0.1
τ_{die}	Parameter	-	0.02	0.05

6.3.1 Simulation with Original Parameters

In this section a simulation using original parameter values is shown, so that the performance of the MHE can be better evaluated. Original parameter values are shown in Table 6.2

Table 6.2: Original parameter values used in the model.

Parameter	Value
h_{front}	$20\,\text{W/m}^2\text{K}$
h_{back}	$60\,\text{W/m}^2\text{K}$
$CF_{\text{k,Al}}$	1
BiasCoil_i, i = 1,2,3,4	$0\,\text{K/s}$
h_{billet}	$40\,\text{W/m}^2\text{K}$
$CF_{\text{viscous dissipation}}$	0.475
$CF_{\text{reduction regions}}$	1
h_{AlAir}	$25\,\text{W/m}^2\text{K}$
h_{AlSteel}	$6000\,\text{W/m}^2\text{K}$
τ_{die}	60 s

Figure 6.6 and 6.7 show the measured and predicted values for the temperatures in the heater. It can be seen that for T_{coil} the predicted values were close to the measurements for coil 1, 2 and 4, while

coil 3 had a significant difference between them. For T_{front} there was some offset between predicted and measured values, but the model managed quite accurate predictions. For T_{back} the difference was large, and the predicted values behaved very differently to the measured values. This might however not entirely be due to model error, as the measurement of T_{back} is deemed unreliable by Hydro. Figure 6.8 shows the four temperature measurements from each billet during transit, and it shows that there was often significant difference between measured and predicted values. In Figure 6.9 one can see that T_{exit} had a significant offset between prediction and measurement, while T_{die} had smaller prediction errors.

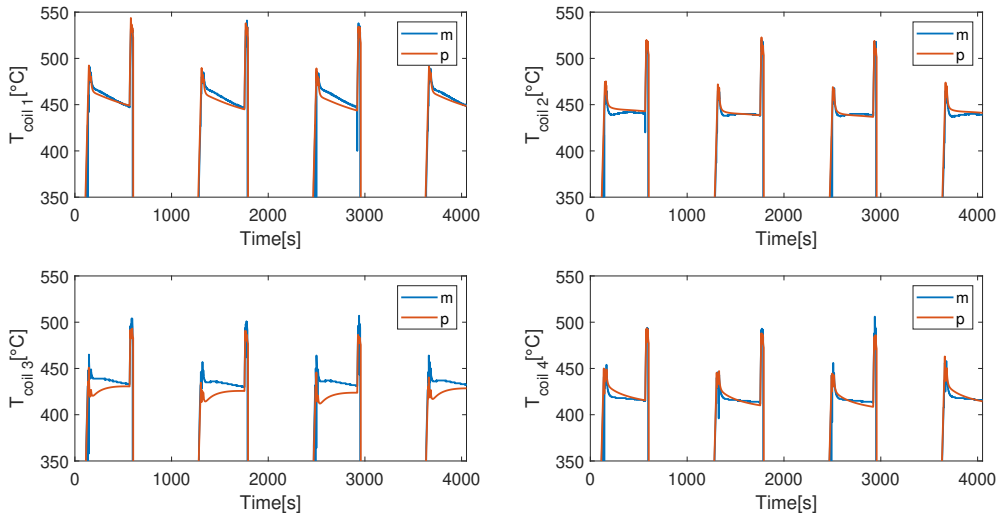

Figure 6.6: Measured (m) and predicted (p) values for the surface temperature of the aluminium billet by each heating coil with original parameter values and without MHE.

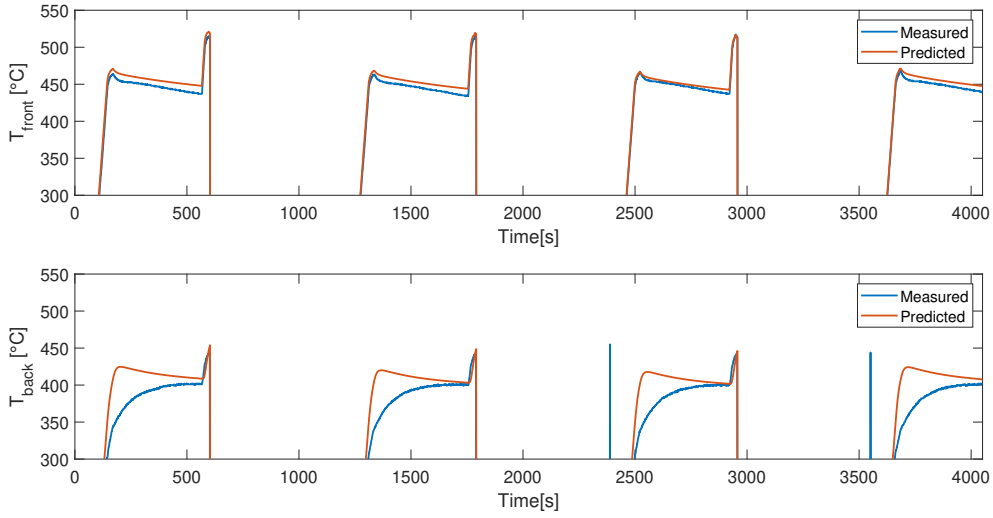

Figure 6.7: Measured and predicted values for the surface temperature of the aluminium billet at the front and back ends with original parameter values and without MHE.

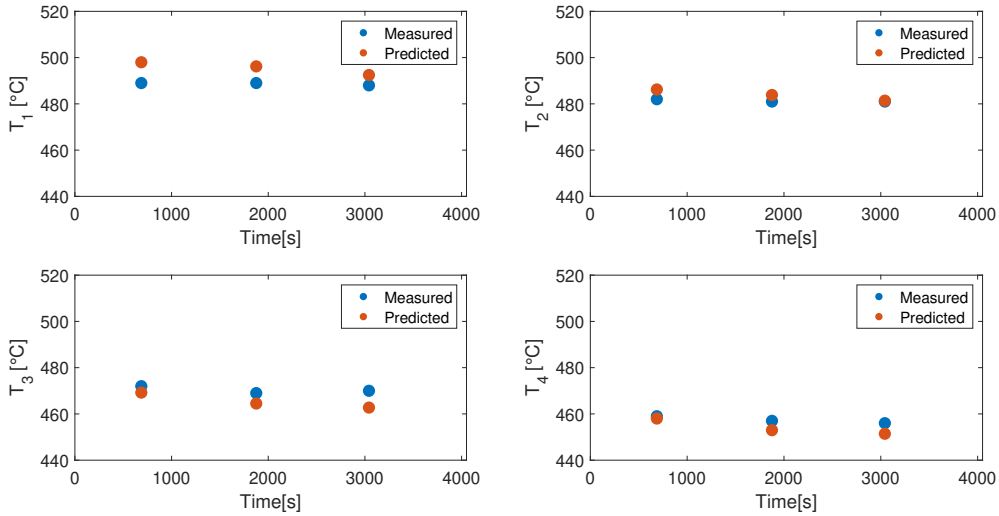

Figure 6.8: Measured and predicted values for the surface temperature of the aluminium billet at the measuring station during transit with original parameter values and without MHE.

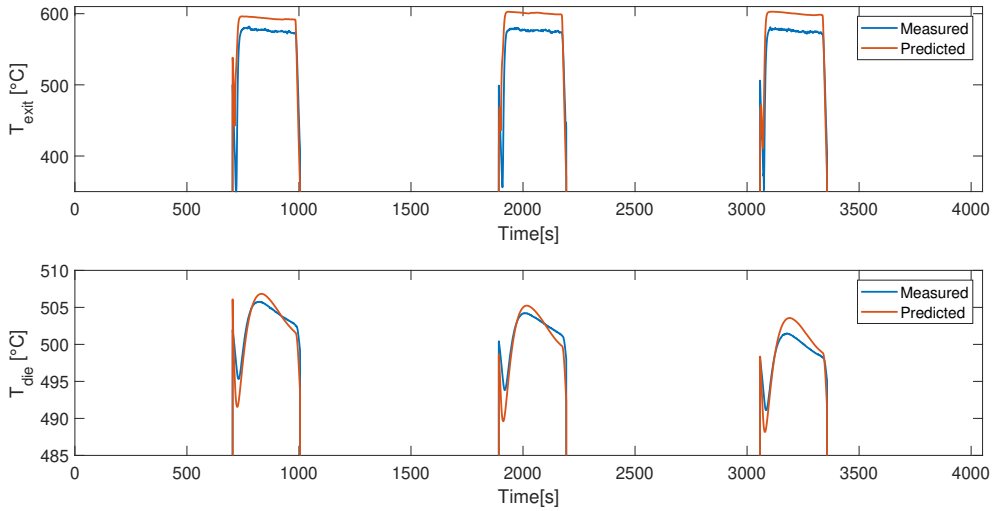

Figure 6.9: Measured and predicted values for T_{die} and T_{exit} during extrusion with original parameter values and without MHE.

6.3.2 Estimate All Parameters

This section presents the results from using MHE on all the model parameters in Table 6.1. The values for the surface temperature of the aluminium billet in the heater are shown in Figure 6.10 and 6.11. They show some improvement for $T_{\text{coil }2}$, $T_{\text{coil }3}$, $T_{\text{coil }4}$ and T_{front}, but $T_{\text{coil }1}$ was a worse fit than before and T_{back} showed no significant improvement. The estimated parameters are shown in Figure 6.12 and 6.13. The bias of the coils, only estimated when the coils are actually on, had quite high variation. Evaluation of what values for the biases are physically reasonable is difficult, but none of the estimates seemed unrealistically high. h_{back} seemed to converge to $80\,\text{W/m}^2\text{K}$ while h_{front} remained quite stable around its initial value. $CF_{\text{k,Al}}$ showed no significant changes. From these results, two changes to the parameter estimation were made:

- The measurement T_{back} was discarded. Information from Hydro and the fact that it fit the model much worse than other measurements indicate that it is not reliable, and it is therefore not useful for parameter estimation.
- $CF_{\text{k,Al}}$ was excluded from the MHE. No significant changes in the parameter value were observed, and it was therefore deemed unnecessary to estimate its value.

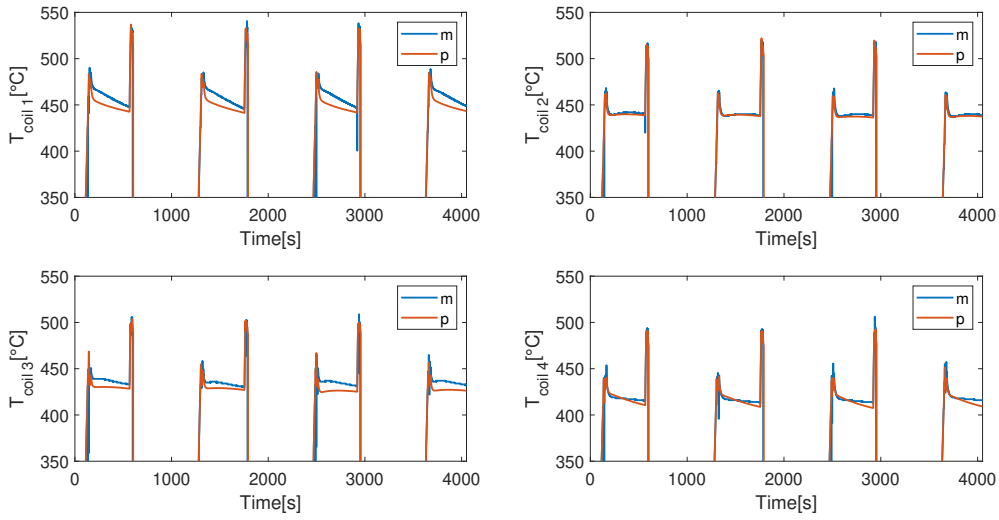

Figure 6.10: Measured (m) and predicted (p) values for the surface temperature of the aluminium billet by each heating coil with MHE on all parameters.

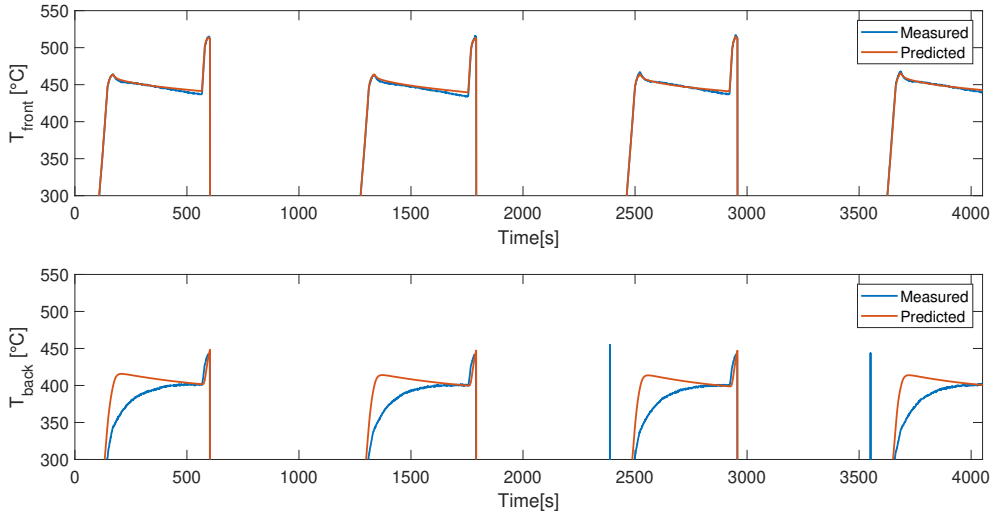

Figure 6.11: Measured and predicted values for the surface temperature of the aluminium billet at the front and back ends with MHE on all parameters.

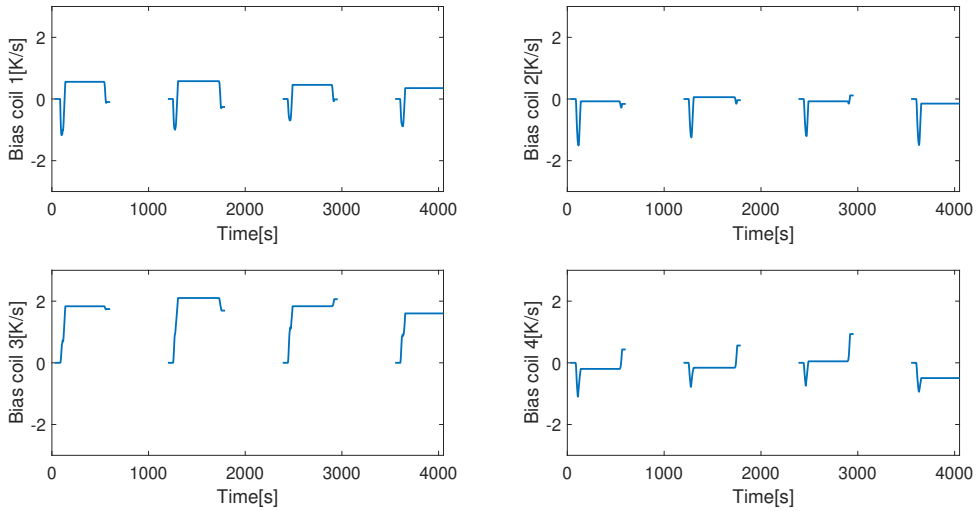

Figure 6.12: Estimated bias for the heating coils with MHE on all parameters.

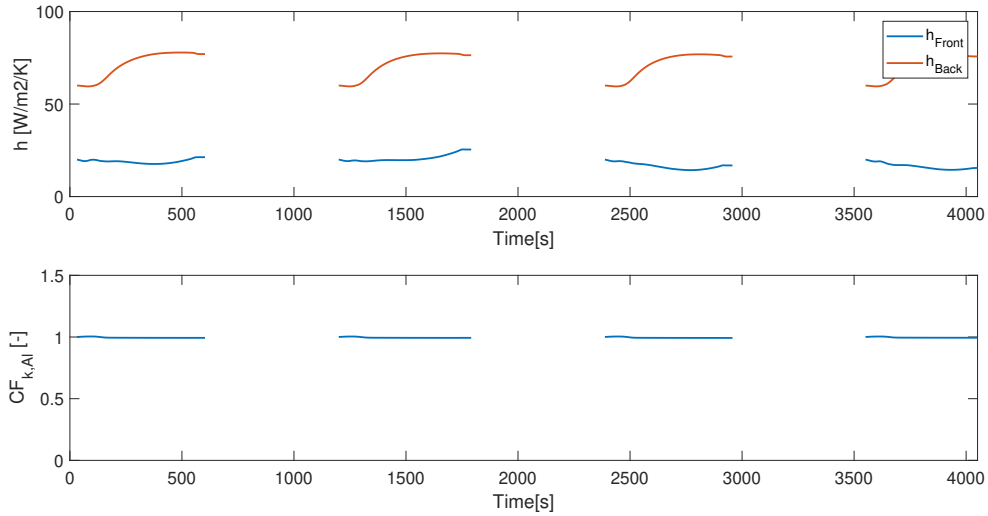

Figure 6.13: Estimated h_{front}, h_{back} and $CF_{\text{k,Al}}$ for the aluminium billet with MHE on all parameters.

Figure 6.14 shows the temperature measurements during transit for the estimation of all the parameters. It shows that the deviation between measured and predicted values was reduced compared to the simulation with no estimation. Figure 6.15 shows that for all three billets the estimated h_{billet} was higher than the initial value. The reason the parameter value changes half way through the transit period is that the parameter cannot be estimated before the billet reaches the measurement station, and thus the initial value must be used by the model for the first part of the transit.

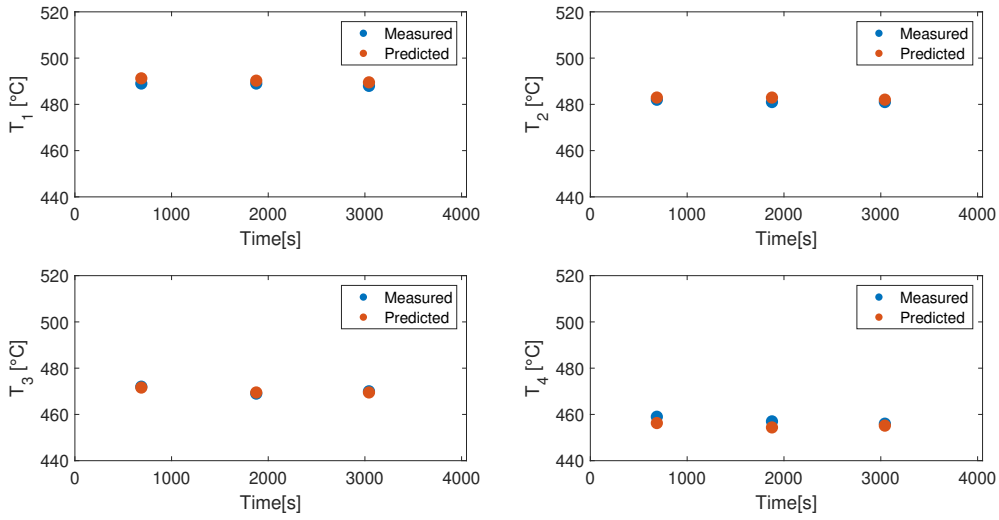

Figure 6.14: Measured and predicted values for the surface temperature of the aluminium billet at the measuring station during transit with MHE on all parameters.

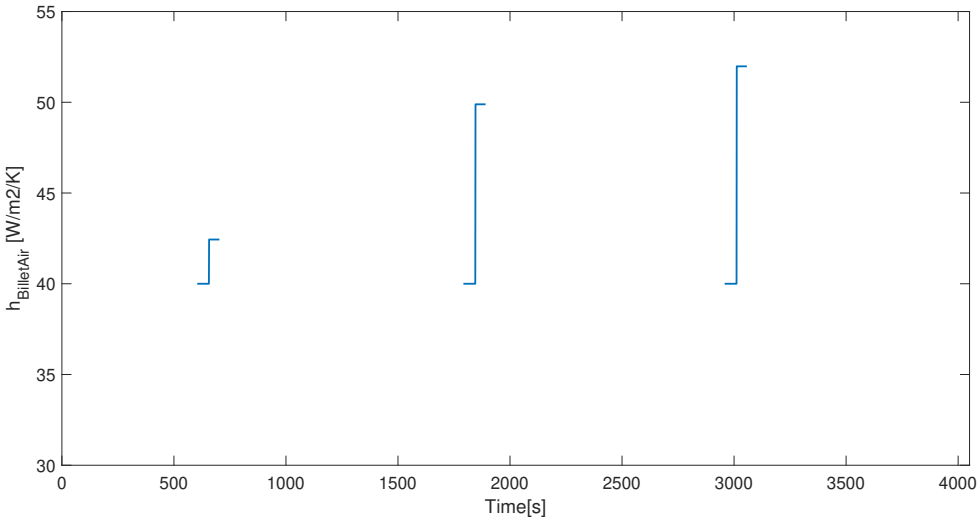

Figure 6.15: Estimated h_{billet} in transit with MHE on all parameters.

The temperature measurements and predictions from the press can be seen in Figure 6.16. They show that both predicted temperatures had some initial deviation from the measurements, but mostly they fit well. The estimated parameters in the extrusion press are shown in Figure 6.17 and 6.18. The correction factor for the heat generated by viscous dissipation showed only very small changes during extrusion. The correction factor for heat generated in the reduction regions was however significantly reduced, and it stabilized around 0.7-0.8 for all three billets. Both the heat transfer coefficients, h_{AlSteel} and h_{AlAir}, were very stable at their initial values, but τ_{die} increased to around 80 s for all three billets and varied some around this value. From these results two changes to the MHE was made:

- h_{AlSteel} was excluded from the MHE, as it was deemed unnecessary to estimate it when it remained approximately at its initial value.
- h_{AlAir} was also excluded from the MHE since it had very little variation. It was also deemed not ideal for estimation. If allowed to vary a lot it could possibly always make the predictions of T_{exit} good, as it determines the heat loss to air after extrusion. This could possibly cover up mistakes in other parameters, which would be bad for the temperature predictions inside the die, which are the most important.

$CF_{\text{viscous dissipation}}$ also varied little, but it was deemed unwise to remove too many parameters at once, as one might lose important information by doing this. It was therefore kept in the MHE until further tests were made.

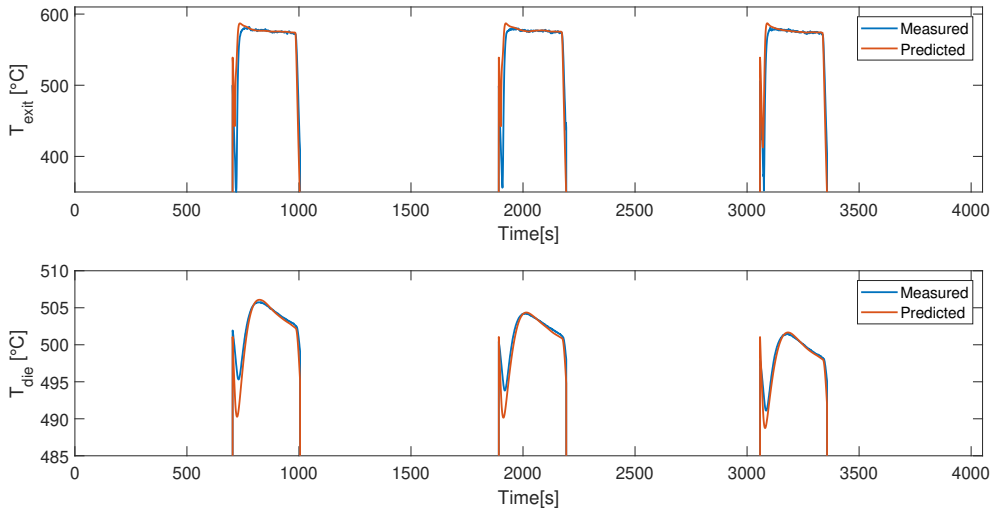

Figure 6.16: Measured and predicted values for T_{die} and T_{exit} during extrusion with MHE on all parameters.

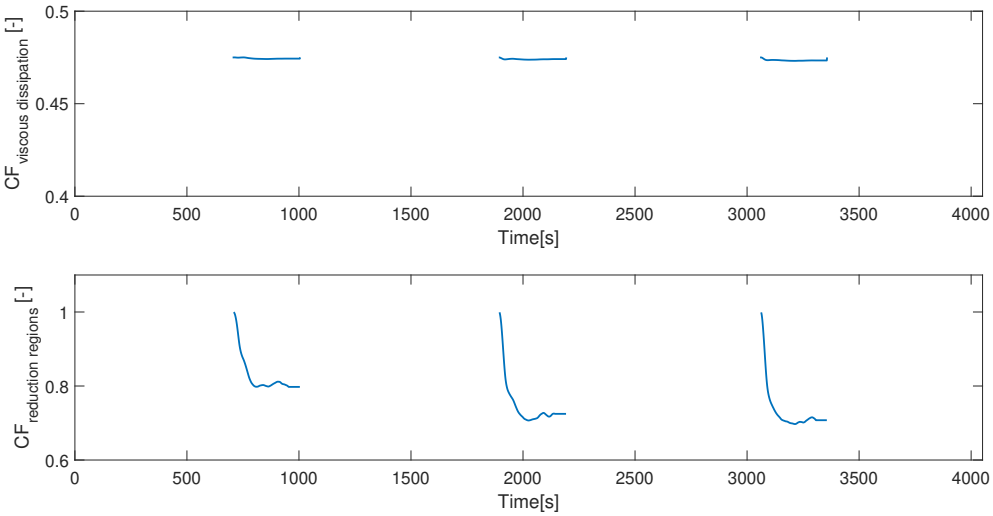

Figure 6.17: Estimated $CF_{\text{viscous dissipation}}$ and $CF_{\text{reduction region}}$ in the extrusion press with MHE on all parameters.

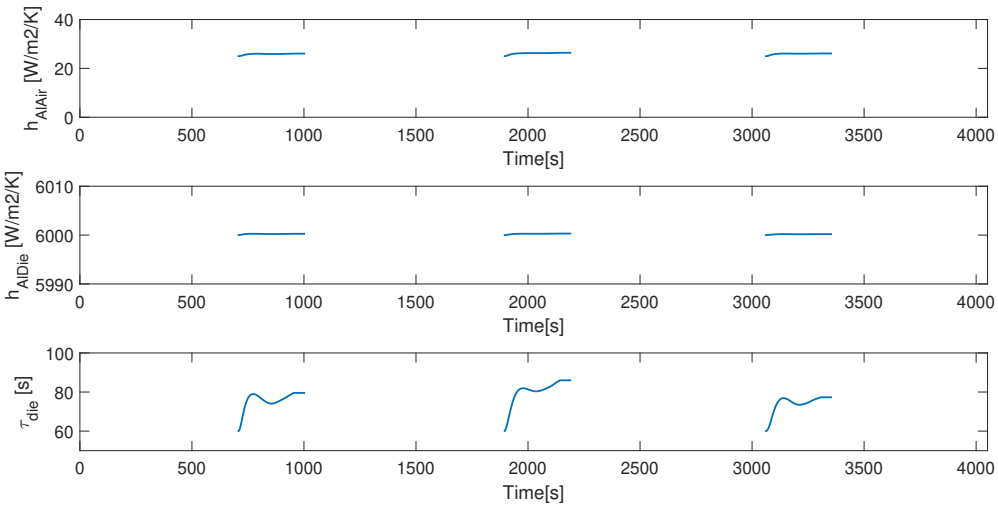

Figure 6.18: Estimated h_{AlAir} and h_{AlSteel} and τ_{die} in the extrusion press with MHE on all parameters.

6.3.3 Constant h_{AlSteel}, h_{AlAir} and $CF_{\text{k,Al}}$. T_{Back} discarded

Figure 6.19 and 6.20 show the temperatures in the heater. No significant changes were observed compared to to simulation with MHE on all parameters, which was described in Section 6.3.2. The estimated parameters are shown in Figure 6.21 and 6.22. The coil biases in Figure 6.21 are very similar to those observed in Section 6.3.2, and the main difference from those results is that h_{back} in Figure 6.22 now remains quite stable a bit above $60\,\text{W/m}^2\text{K}$ instead of increasing to $80\,\text{W/m}^2\text{K}$. This is most likely a result of the measurement T_{back} being discarded. In addition, the variations in h_{front} were a bit higher than before.

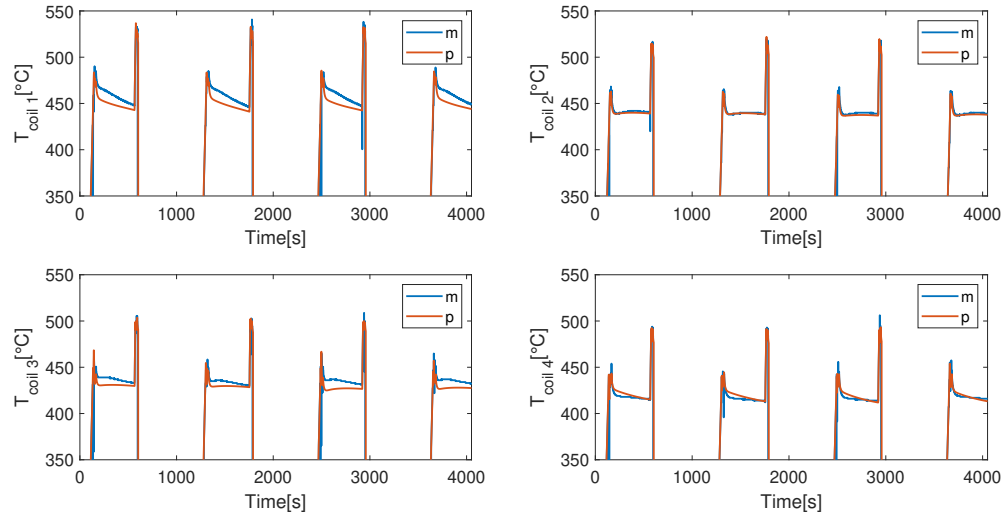

Figure 6.19: Measured (m) and predicted (p) values for the surface temperature of the aluminium billet by each heating coil with MHE without h_{AlSteel}, h_{AlAir}, $CF_{\text{k,Al}}$ and T_{Back}.

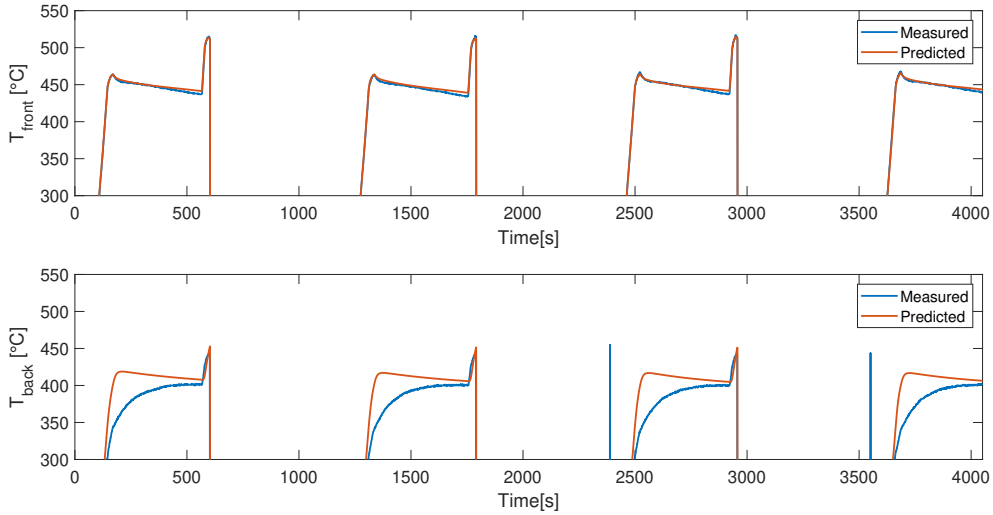

Figure 6.20: Measured and predicted values for the surface temperature of the aluminium billet at the front and back ends with MHE without h_{AlSteel}, h_{AlAir}, $CF_{\text{k,Al}}$ and T_{Back}.

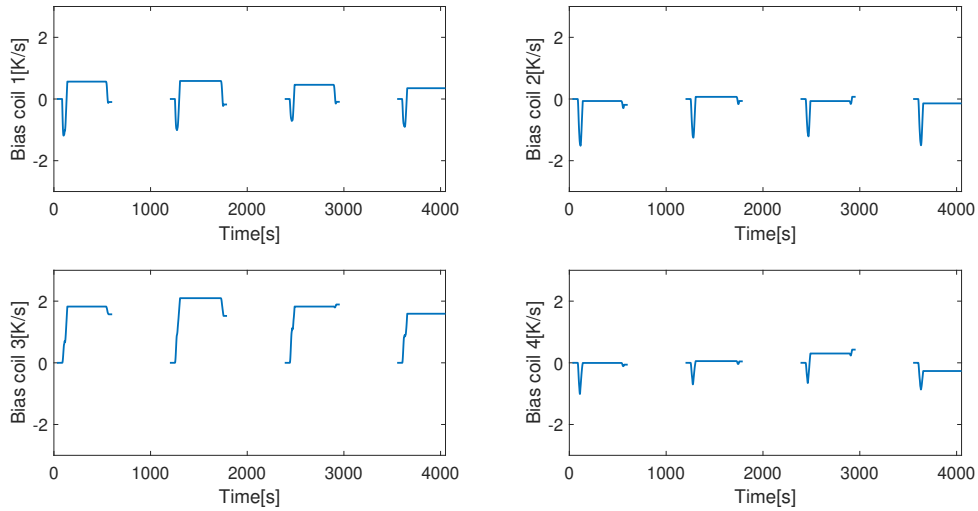

Figure 6.21: Estimated bias for the heating coils with MHE without h_{AlSteel}, h_{AlAir}, $CF_{\text{k,Al}}$ and T_{Back}.

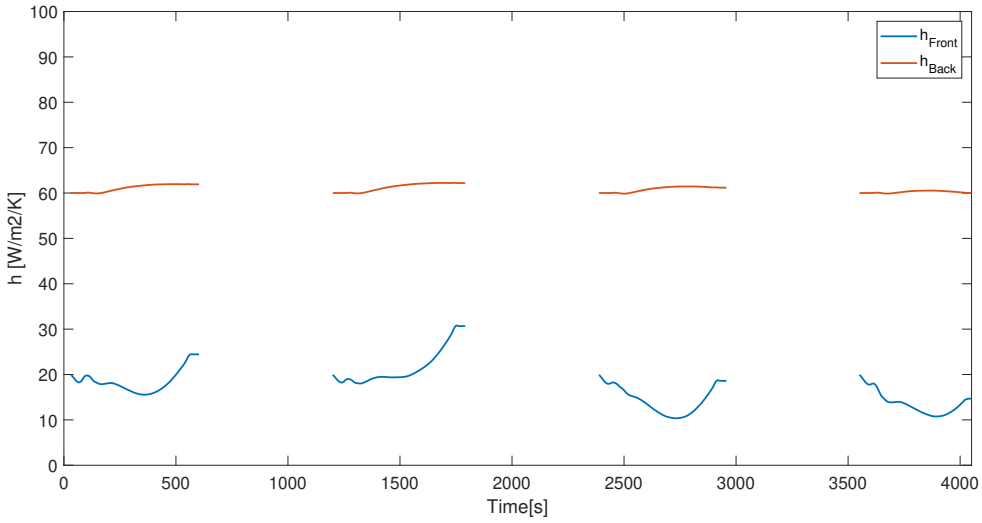

Figure 6.22: Estimated h_{front}, h_{back} and $CF_{\text{k,Al}}$ for the aluminium billet with MHE without h_{AlSteel}, h_{AlAir}, $CF_{\text{k,Al}}$ and T_{Back}.

Figure 6.23 shows the temperature measurements and predictions during transit. No observable difference from MHE with all parameters was observed. Some difference was however apparent for the estimated heat transfer coefficient in Figure 6.24. New estimates for the parameter were higher than before, which is probably due to slightly different temperatures in the heater with new parameter estimates. Based on this the following change was made:

- The initial value of h_{billet} was increased from $40\,\text{W/m}^2\text{K}$ to $45\,\text{W/m}^2\text{K}$, as estimated values in the simulations always had been higher than the initial guess. It was not set higher than $45\,\text{W/m}^2\text{K}$ since it was expected that the too low initial guess resulted in too high estimated values to compensate for too little heat loss in the start of the transit period.

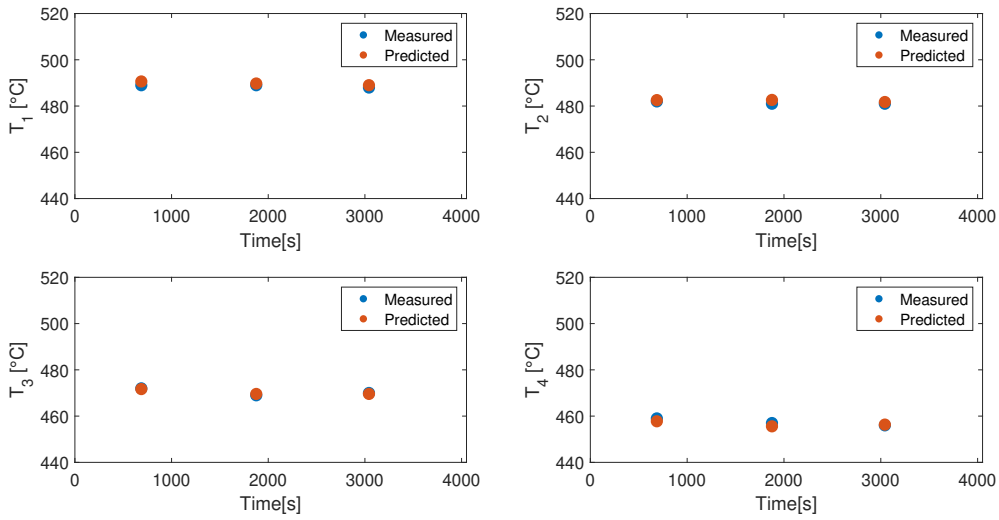

Figure 6.23: Measured and predicted values for the surface temperature of the aluminium billet at the measuring station during transit with MHE without h_{AlSteel}, h_{AlAir}, $CF_{\text{k,Al}}$ and T_{Back}.

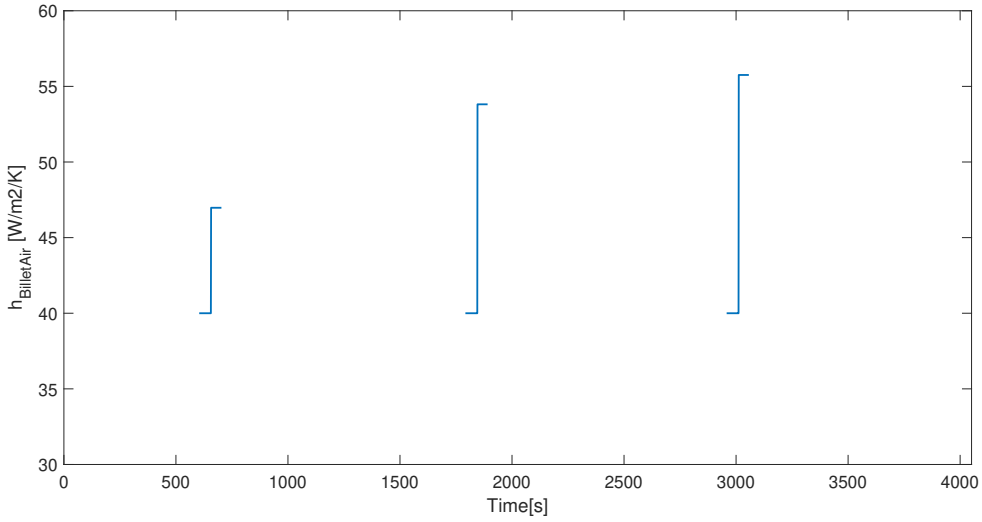

Figure 6.24: Estimated h_{billet} in transit with MHE without h_{AlSteel}, h_{AlAir}, $CF_{\text{k,Al}}$ and T_{Back}.

Figure 6.25 shows measured and predicted temperatures in the press with constant values for h_{AlSteel} and h_{AlAir}. No differences from the plot with MHE on all parameters, shown in Figure 6.16, can be observed. This is to be expected, as h_{AlSteel} and h_{AlAir} varied very little during the previous estimation. The behaviour of the estimated parameters shown in Figure 6.26 was also the same as in the MHE of all parameters. Based on these results, the following conclusions were drawn:

- $CF_{\text{viscous dissipation}}$ should not be included in the MHE, as its value changes only negligible amounts.
- The initial value of $CF_{\text{reduction regions}}$ should be changed to 0.7, as this is approximately where the estimated value lies during extrusion.

- The initial value of τ_{die} should be set to 80 s, as the estimated value varies around this point during extrusion.

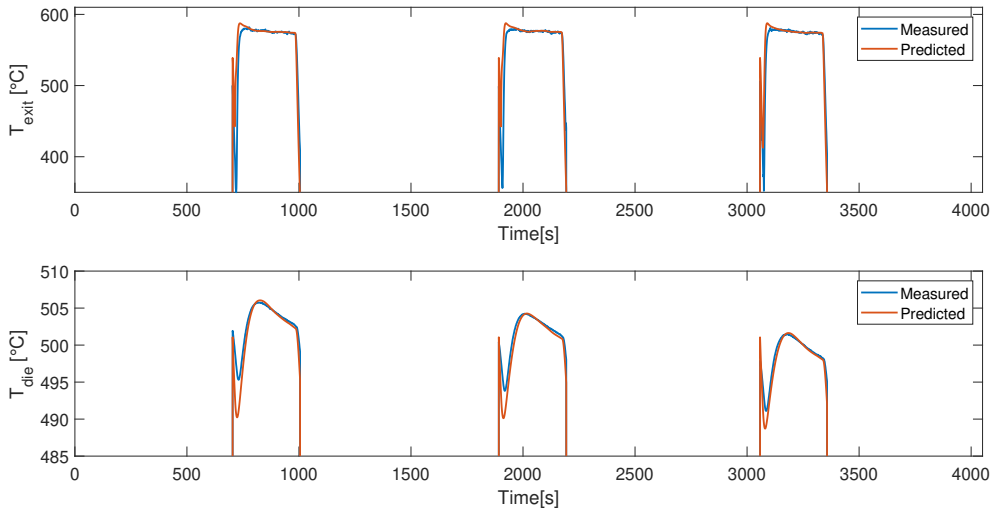

Figure 6.25: Measured and predicted values for T_{die} and T_{exit} during extrusion with MHE without h_{AlSteel}, h_{AlAir}, $CF_{\text{k,Al}}$ and T_{Back}.

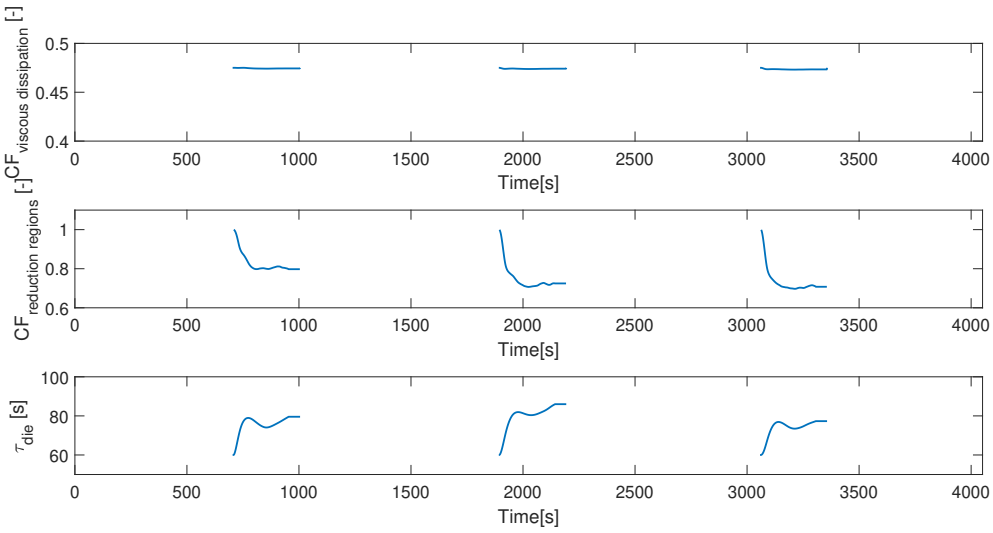

Figure 6.26: Estimated $CF_{\text{viscous dissipation}}$, $CF_{\text{reduction region}}$ and τ_{die} in the extrusion press with MHE without h_{AlSteel}, h_{AlAir}, $CF_{\text{k,Al}}$ and T_{Back}.

6.3.4 Constant $CF_{\text{viscous dissipation}}$ and New Initial Guesses

This section presents the results from the parameter estimation with constant h_{AlSteel}, h_{AlAir}, $CF_{\text{k,Al}}$, $CF_{\text{viscous dissipation}}$ and T_{Back} not included in the MHE and updated initial values for h_{billet}, $CF_{\text{reduction regions}}$ and τ_{die}. Simulations from the heater part of the model are not shown here, since no changes were made to the estimation in this part of the model. The temperatures and parameters in the heater were therefore identical to those presented in Section 6.3.3. Figure 6.27 shows the temperatures in transit. As in previous simulations there was very little prediction error. The estimated heat transfer coefficient with the new initial value, showed in Figure 6.28, was now a bit lower than when the initial value was lower. This indicates that the assumption that the estimates were too high from Section 6.3.3 was correct. Some of the new estimates were below the initial value, while others were above, indicating that the new initial guess is a good starting point for estimation.

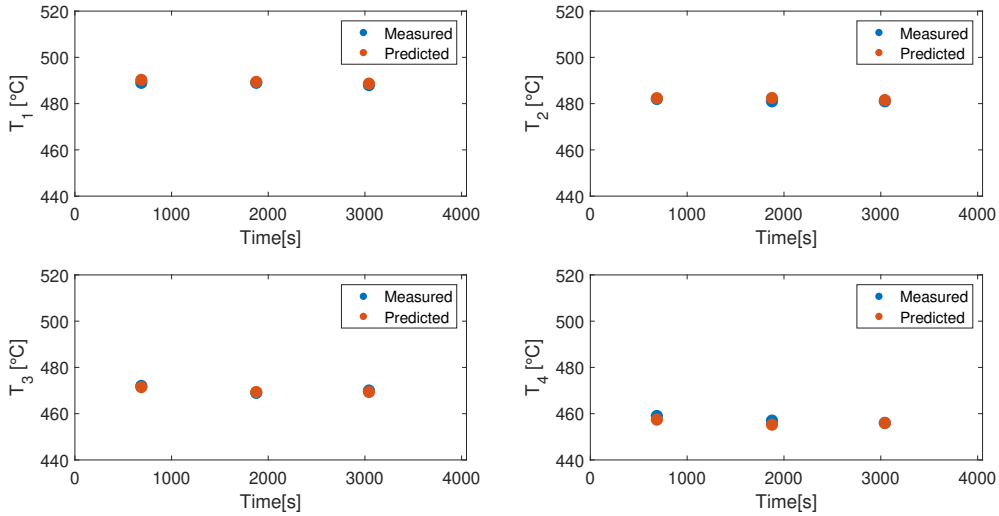

Figure 6.27: Measured and predicted values for the surface temperature of the aluminium billet at the measuring station during transit with MHE without h_{AlSteel}, h_{AlAir}, $CF_{\text{k,Al}}$, $CF_{\text{viscous dissipation}}$ and T_{Back} and new initial values for h_{billet}, $CF_{\text{reduction regions}}$ and τ_{die}.

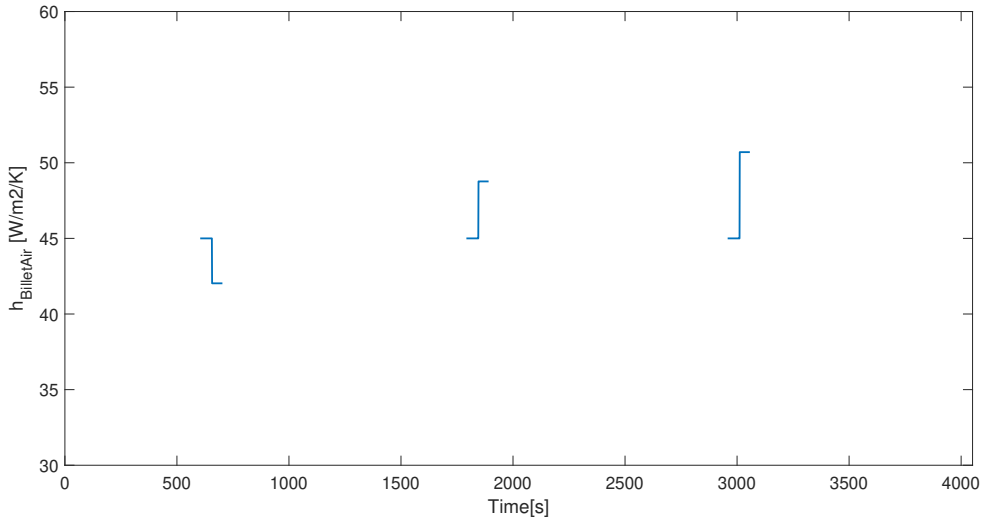

Figure 6.28: Estimated h_{billet} in transit with MHE without h_{AlSteel}, h_{AlAir}, $CF_{\text{k,Al}}$, $CF_{\text{viscous dissipation}}$ and T_{Back} and new initial values for h_{billet}, $CF_{\text{reduction regions}}$ and τ_{die}.

Figure 6.29 shows the temperatures in the press. Compared to the results presented in Section 6.3.3 the initial behaviour of T_{exit} has improved. The overshoot in the predicted values at the start of the extrusion cycle was not present any more. For T_{die} the initial undershoot was reduced, and apart from a small temperature overshoot in the first billet the prediction error for the later part of the cycles was just as good as before. The new initial values for $CF_{\text{reduction regions}}$ and τ_{die} therefore seem to have reduced the error en the predictions. Figure 6.30 shows that the estimated parameters behaved similarly to the results in Section 6.3.3. The starting points for the estimation were different, but $CF_{\text{reduction regions}}$ still stabilized around 0.7 - 0.8 and τ_{die} still varied around 80 s. The removal of $CF_{\text{viscous dissipation}}$ from the MHE did therefore not seem to affect the other estimated parameters.

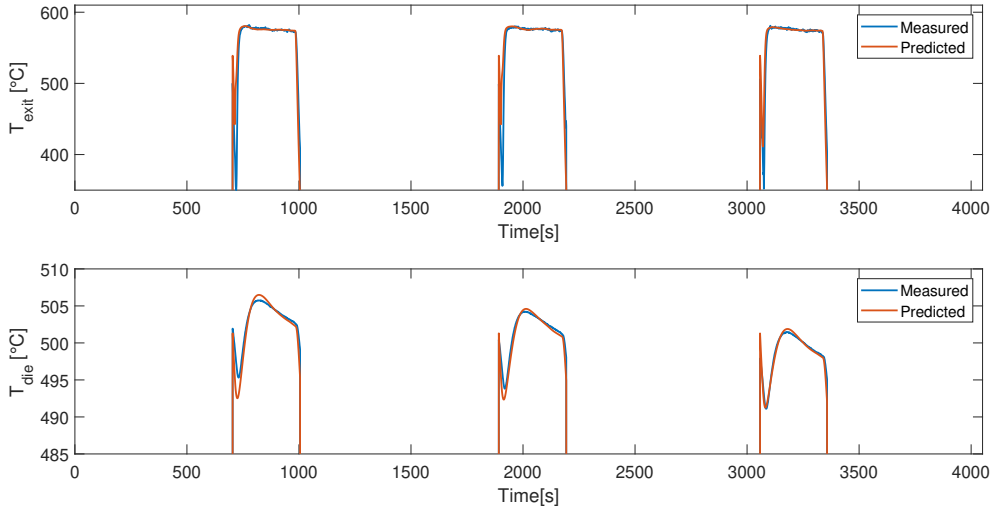

Figure 6.29: Measured and predicted values for T_{die} and T_{exit} during extrusion with MHE without h_{AlSteel}, h_{AlAir}, $CF_{\text{k,Al}}$, $CF_{\text{viscous dissipation}}$ and T_{Back} and new initial values for h_{billet}, $CF_{\text{reduction regions}}$ and τ_{die}.

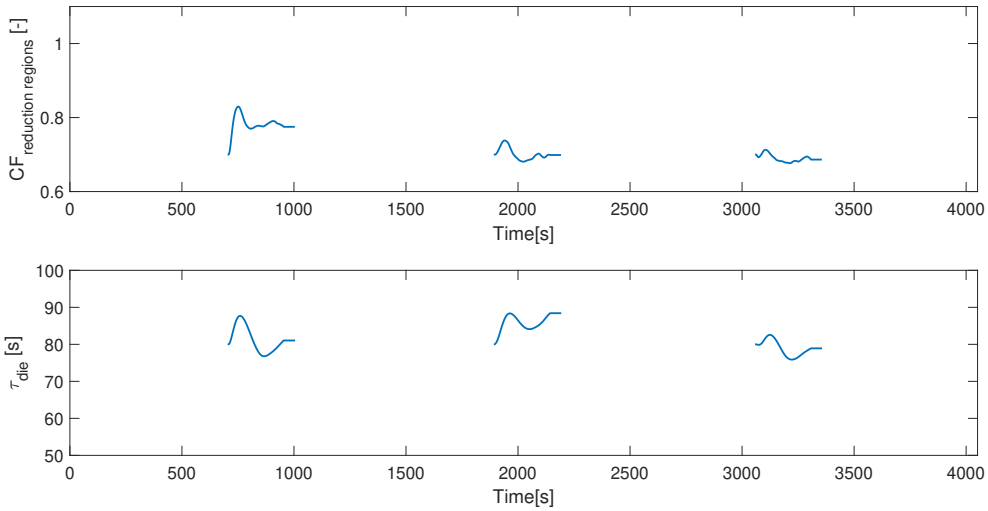

Figure 6.30: Estimated $CF_{\text{reduction region}}$ and τ_{die} in the extrusion press with MHE without h_{AlSteel}, h_{AlAir}, $CF_{\text{k,Al}}$, $CF_{\text{viscous dissipation}}$ and T_{Back} and new initial values for h_{billet}, $CF_{\text{reduction regions}}$ and τ_{die}.

6.3.5 Lower Measurement Noise in Heater

From previous simulations of the heater, shown in Section 6.3.2 and 6.3.3, only the predictions for T_{front} and $T_{\text{coil 2}}$ managed to fit measurements very well. The rest of the temperatures had significant offsets. To investigate if these offsets could be reduced a set of different tuning parameters for the MHE in the heater was tested. The previous tunings are described in Table 6.1. To reduce the offset in the heater the values in the matrix W in Equation 5.1 corresponding to the temperature measurements in the heater were reduced from 1 to 0.1. This means the MHE weighted reducing the prediction error for these measurements more than before, possibly resulting in larger changes in the estimated parameters. In this estimation the parameter $CF_{\text{k,Al}}$ was included in the MHE again to allow it more degrees of freedom to fit the predictions. The resulting temperatures from this simulation are shown in Figure 6.31 and 6.32. The plots show some improvement for $T_{\text{coil 1}}$, $T_{\text{coil 3}}$ and $T_{\text{coil 4}}$, but $T_{\text{coil 2}}$ fit worse than before. T_{front} was still as good as previous simulations, and T_{back} was a bit closer to the measured values even though it was not included in the MHE. These small improvements did however require very high variations in some parameters. The coil bias in Figure 6.33 behaved similarly to previous simulations, but the heat transfer coefficients in Figure 6.34 had much higher variability than is physically reasonable. The change in $CF_{\text{k,Al}}$ was also higher than before, but not as extreme as for the heat transfer coefficients. This non-physical behaviour suggests that the model might not fit the heater well enough due to unmodeled factors affecting the billet temperature, or because the measurements were inaccurate. As the measurement of T_{back} already has been discarded due to suspected inaccuracy, it is not improbable that other measurements also have problems. One unmodeled/unmeasured factor that could contribute to the lack of fit of the model is the air temperature T_a around the billet in the heater. This is not measured and is assumed constant at 20 °C in the model, which is probably an inaccurate assumption as the air in the heater is not exchanged rapidly, meaning the temperature is likely to rise. This would affect the heat loss from the surface, and the non-physical behaviour of the heat transfer coefficients could be a result of this. Another assumption which might contribute to the lack of fit is that the model only considers heat loss from the billet ends. Zero heat loss is therefore assumed for the surface where T_{coil} is measured, which could explain why the model struggles to predict these temperatures accurately. The low improvement in model predictions and low stability of estimated heat transfer coefficients makes the updated values

in W undesirable, and the original values of 1 should be kept.

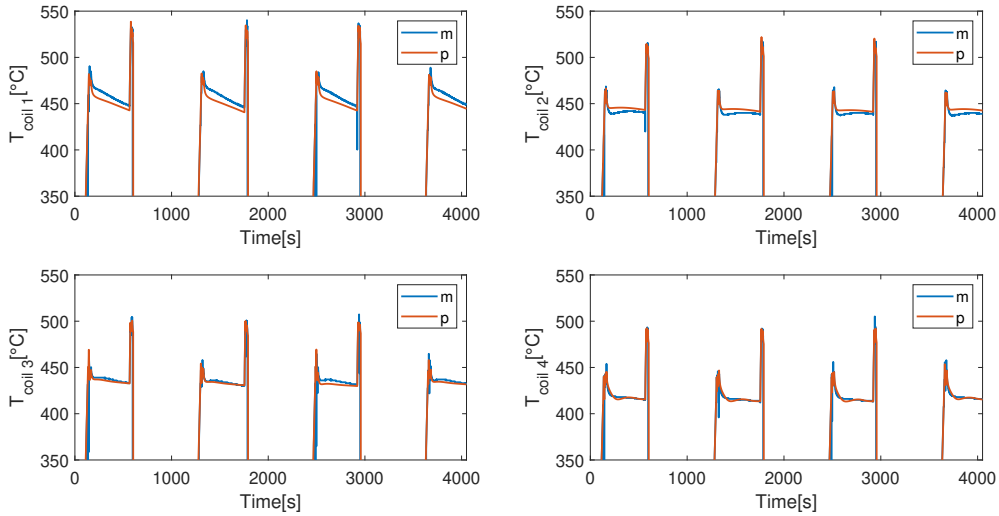

Figure 6.31: Measured (m) and predicted (p) values for the surface temperature of the aluminium billet by each heating coil with MHE with lower measurement noise in the heater.

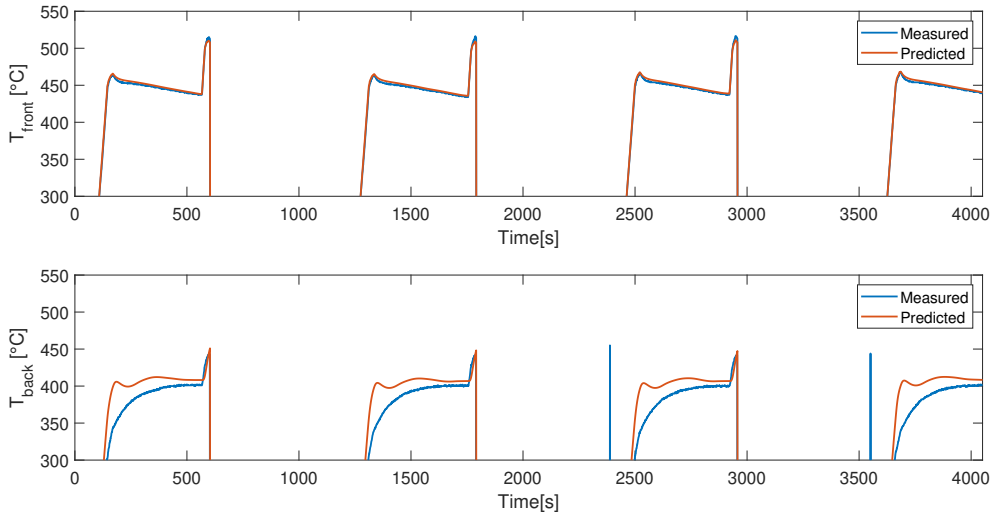

Figure 6.32: Measured and predicted values for the surface temperature of the aluminium billet at the front and back ends with MHE with lower measurement noise in the heater.

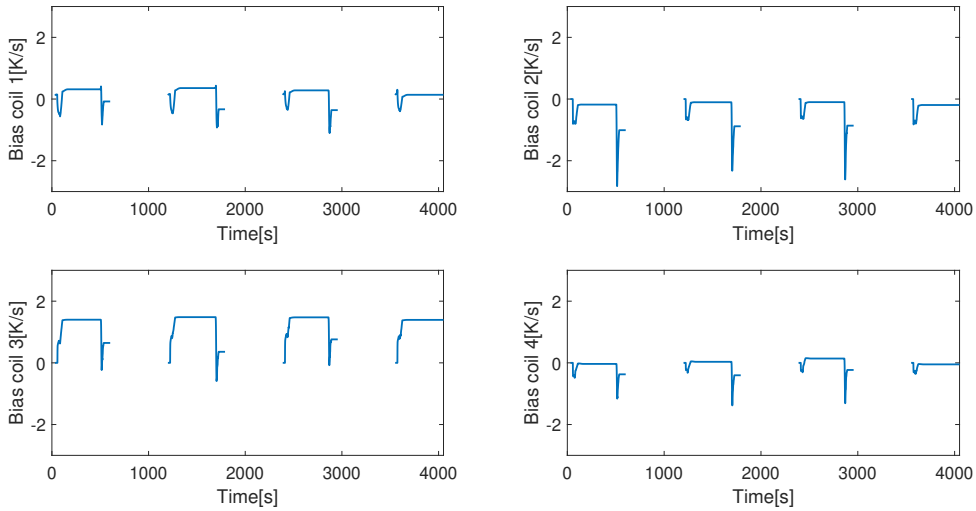

Figure 6.33: Estimated bias for the heating coils with MHE with lower measurement noise in the heater.

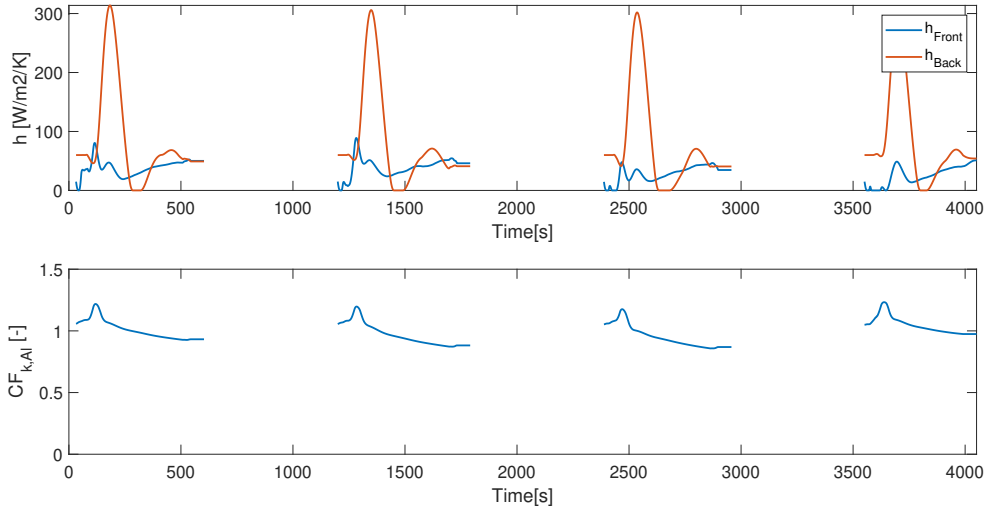

Figure 6.34: Estimated h_{front}, h_{back} and $CF_{\text{k,Al}}$ for the aluminium billet with MHE with lower measurement noise in the heater.

6.3.6 Longer Estimation Horizon

A longer estimation horizon was also tested to see if this would improve model predictions. Originally, a horizon of $N_T = 30$ samples was used. In this section estimation with $N_T = 60$ was tested. The resulting temperatures in the heater are shown in Figure 6.35 and 6.36. They showed no significant difference from the results of MHE using $N_T = 30$ and identical tuning, which was presented in Section 6.3.3. Some difference can be observed in the plot of coil bias in Figure 6.37. The new estimates had lower values than with $N_T = 30$. For the heat transfer coefficients in Figure 6.38 the variation in the estimates was higher than before, but as this resulted in no significant improvements in the predictions

the higher N_T was not considered to have improved MHE performance in the heater.

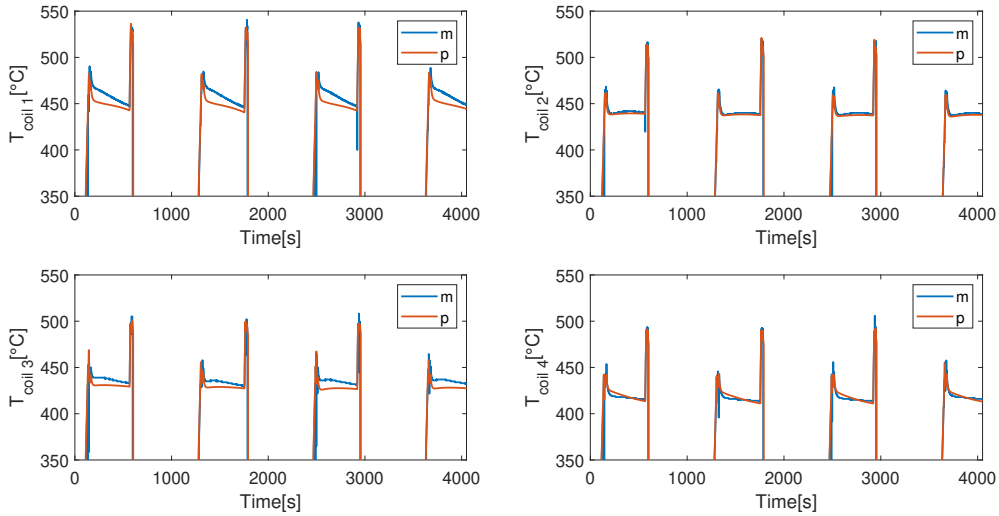

Figure 6.35: Measured (m) and predicted (p) values for the surface temperature of the aluminium billet by each heating coil with MHE with $N_T = 60$.

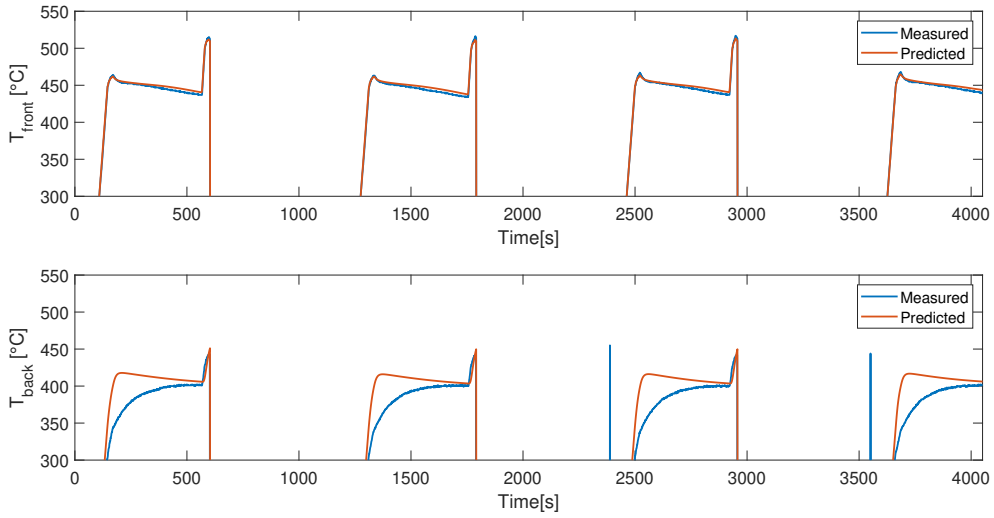

Figure 6.36: Measured and predicted values for the surface temperature of the aluminium billet at the front and back ends with MHE with $N_T = 60$.

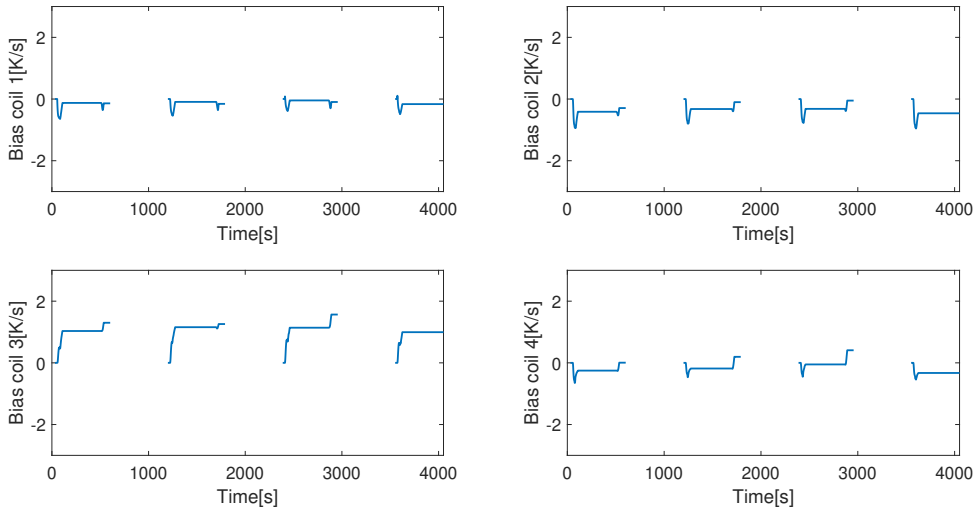

Figure 6.37: Estimated bias for the heating coils with MHE with $N_T = 60$.

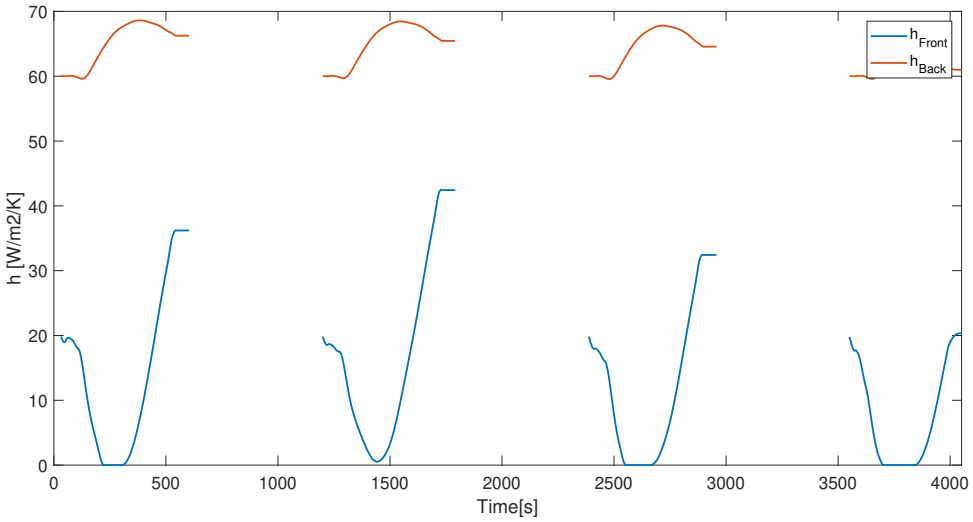

Figure 6.38: Estimated h_{front} and h_{back} for the aluminium billet with MHE with $N_T = 60$.

The temperatures in transit, shown in Figure 6.39, showed no difference from simulations with $N_T = 30$ shown in Section 6.3.4. The new estimates of h_{billet} shown in Figure 6.40 were lower than the previous results, but since these estimates are only made from measurements at 1 point in time the difference is most likely due to small differences in the billet temperature in the heater, since the estimation was made on the same data point in both cases.

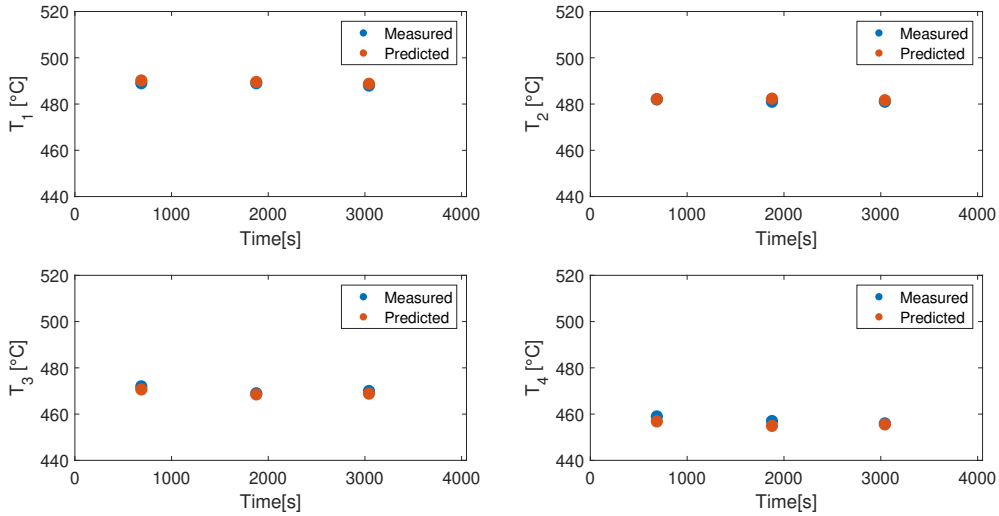

Figure 6.39: Measured and predicted values for the surface temperature of the aluminium billet at the measuring station during transit with MHE with $N_T = 60$.

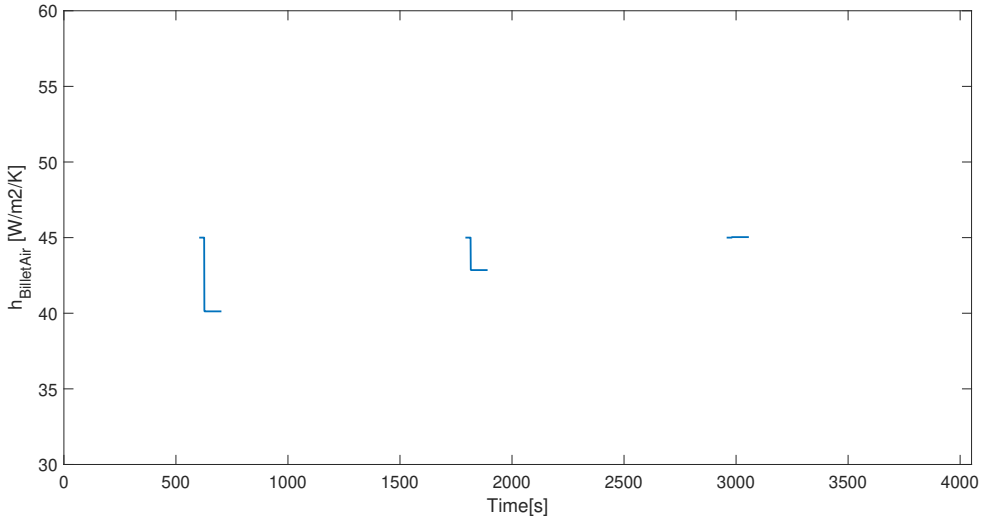

Figure 6.40: Estimated h_{billet} in transit with MHE with $N_T = 60$.

The temperatures in the press are shown in Figure 6.41. They showed some improvement from simulations with $N_T = 30$, and apart from small initial undershoots of T_{die} no significant difference between measured and predicted temperatures can be observed for either T_{die} or T_{exit}. The parameter estimates shown in Figure 6.42 were quite similar to previous result, the main difference being that the new estimates of $CF_{\text{reduction region}}$ were more stable than before. The small improvement in prediction accuracy when using longer N_T was however accompanied by an increased computational cost. To accept this extra cost the new parameter estimates would have do be significantly better than the ones made with a shorter N_T. Here, the difference was small, and estimation with $N_T = 30$ was therefore deemed accurate enough.

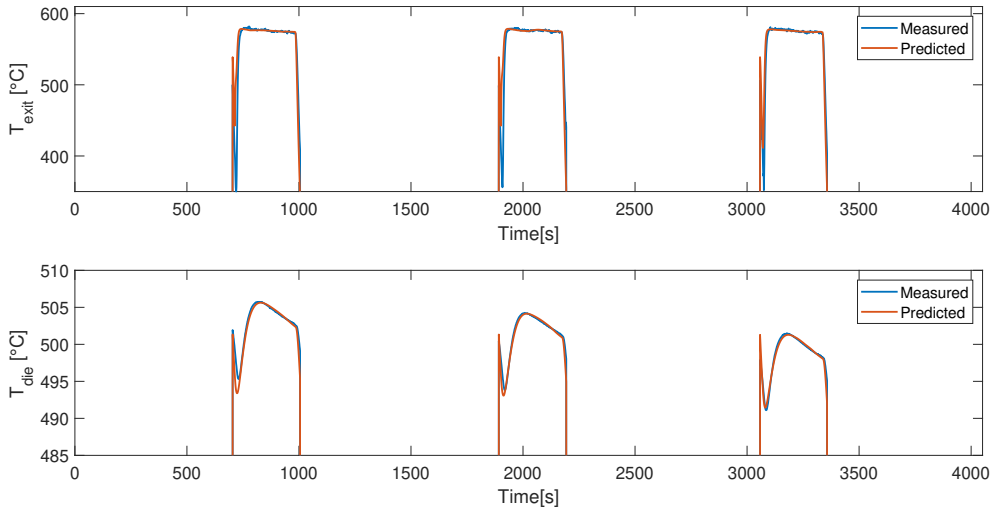

Figure 6.41: Measured and predicted values for T_{die} and T_{exit} during extrusion with MHE with $N_T = 60$.

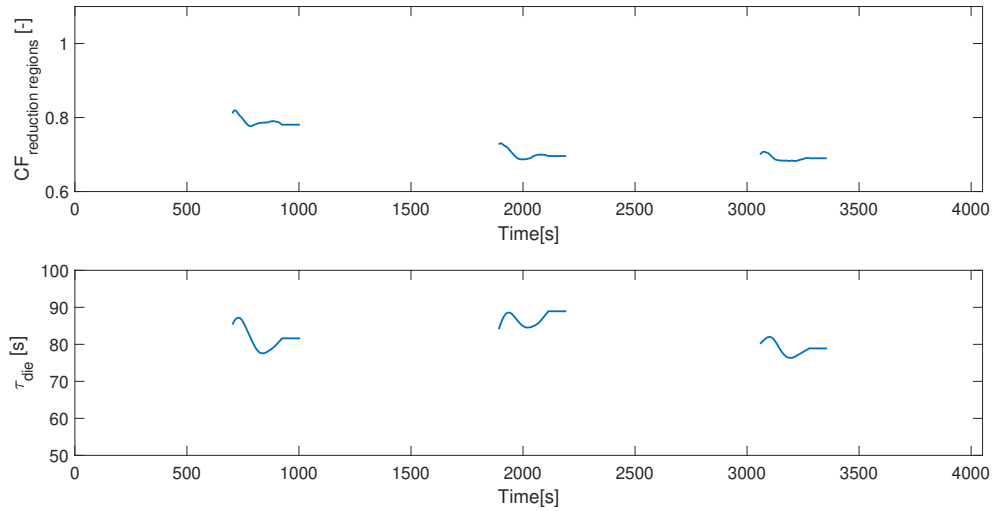

Figure 6.42: Estimated $CF_{\text{reduction region}}$ and τ_{die} in the extrusion press with MHE with $N_T = 60$.

6.3.7 Longer Data Series

The development of the parameter estimation was done based on a data series containing three full extrusion cycles. To check that the MHE worked on data not used to develop it, it was tested on a longer data set. The MHE variant considered to be the best in this project was the one described in Section 6.3.4, as it was deemed to give both good predictions and stable parameter estimates at a low computational cost. The resulting temperatures in the heater are shown in Figure 6.43 and 6.44. The three first billets in the plot are the ones used in the previous simulation, and it can be seen that the accuracy of the predictions was similar for later billets. The behaviour of the estimated parameters in Figure 6.45 and 6.46 was also similar for the rest of the data set.

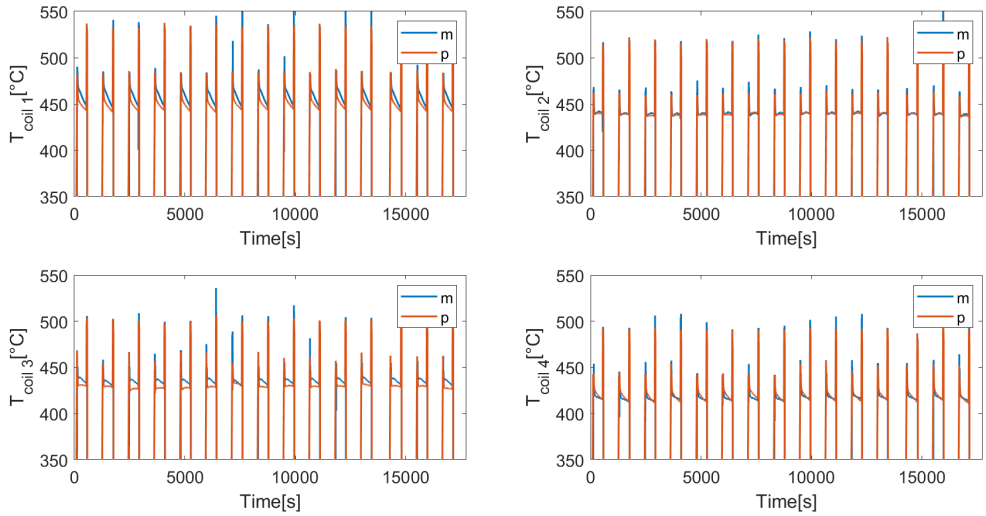

Figure 6.43: Measured (m) and predicted (p) values for the surface temperature of the aluminium billet by each heating coil with MHE with a longer data series.

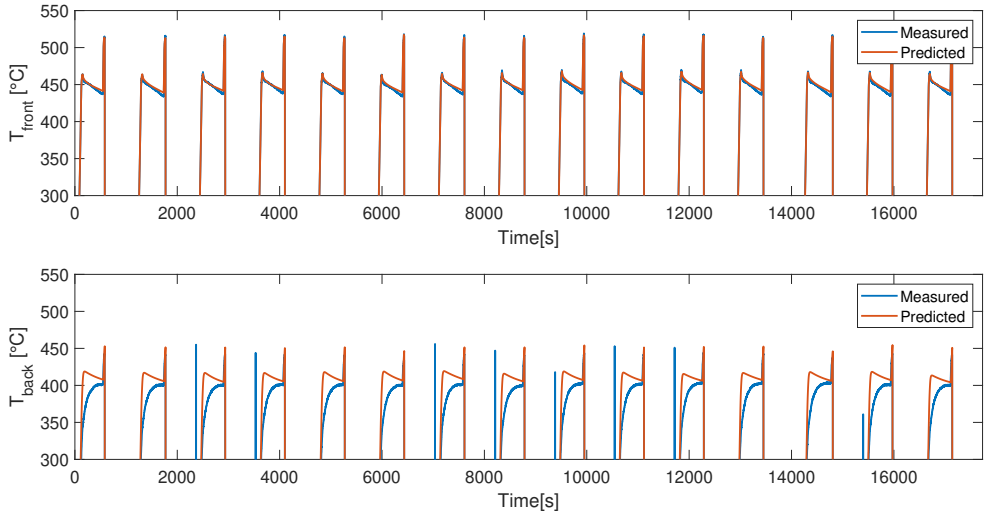

Figure 6.44: Measured and predicted values for the surface temperature of the aluminium billet at the front and back ends with MHE with a longer data series.

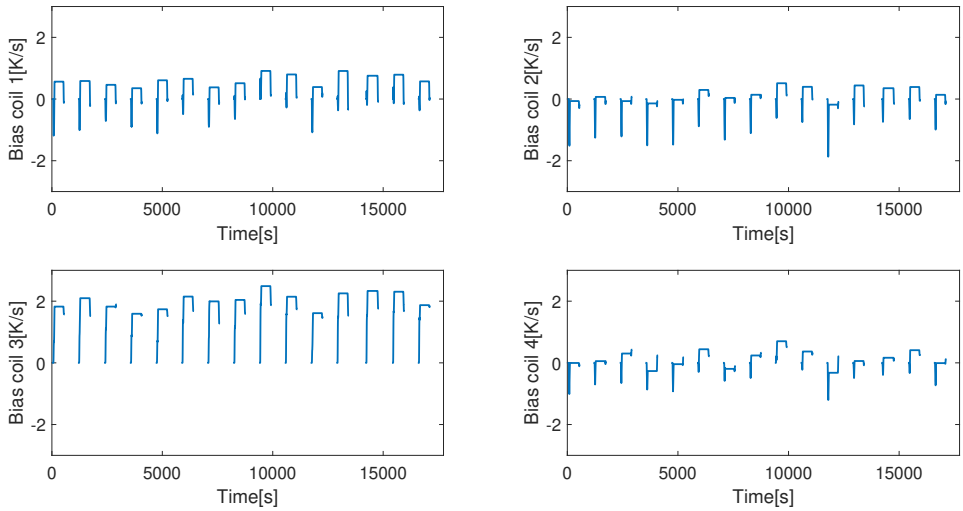

Figure 6.45: Estimated bias for the heating coils with MHE with a longer data series.

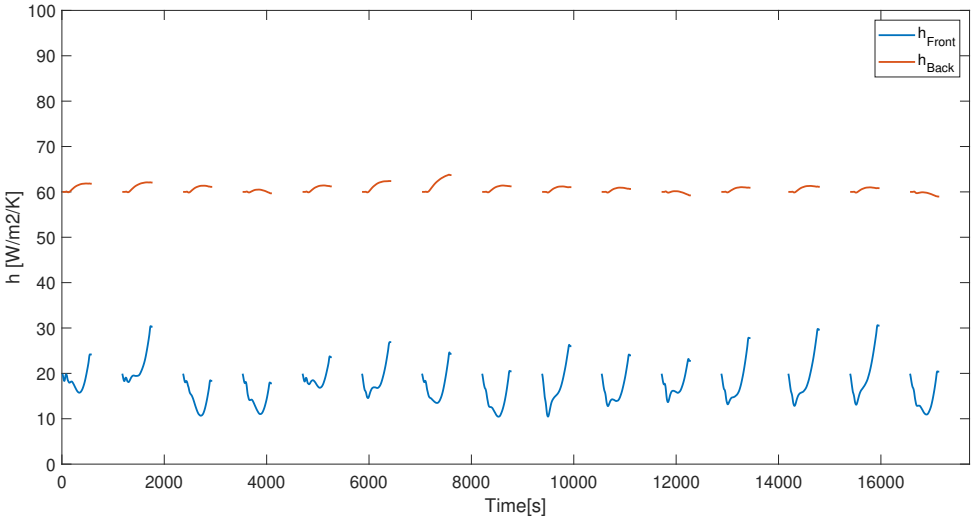

Figure 6.46: Estimated h_{front} and h_{back} for the aluminium billet with MHE with a longer data series.

For the transit model, the temperatures in Figure 6.47 showed that the predictions were accurate for the new data sat as well. The behaviour of h_{billet} did however differ later in the data series. Estimated values were there often significantly lower than before, suggesting that the new initial value of $45\,\text{W/m}^2\text{K}$ might be too high. The estimation was therefore retried with the old initial value $40\,\text{W/m}^2\text{K}$. The resulting parameter estimates are shown in Figure 6.49, and they show that new estimates varied approximately as much as before. This is probably due to the estimate being made from measurements at only one point in time, which makes them more affected by uncertainties in the measurements. Due to this lack of data it was therefore deemed unrealistic to gain a better estimate of h_{billet}, and the original value of $40\,\text{W/m}^2\text{K}$ was kept.

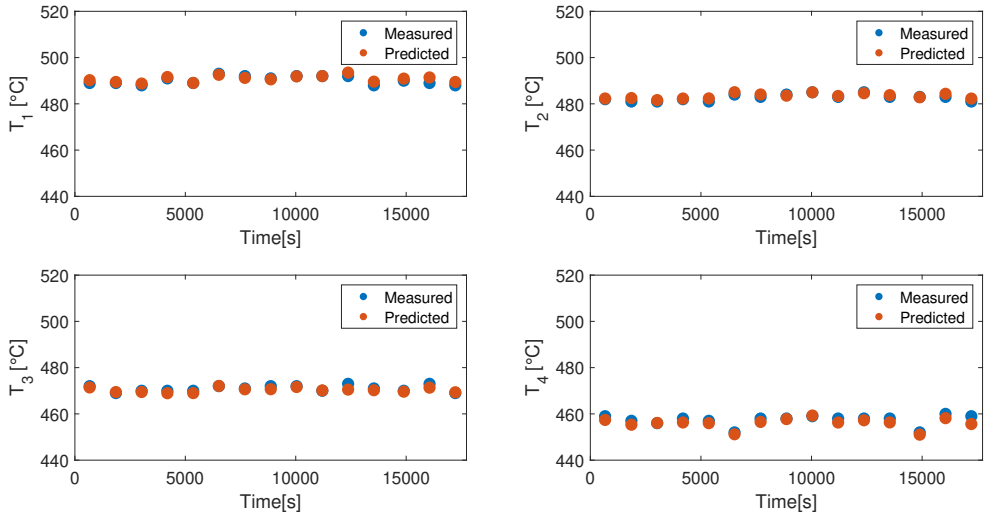

Figure 6.47: Measured and predicted values for the surface temperature of the aluminium billet at the measuring station during transit with MHE with a longer data series.

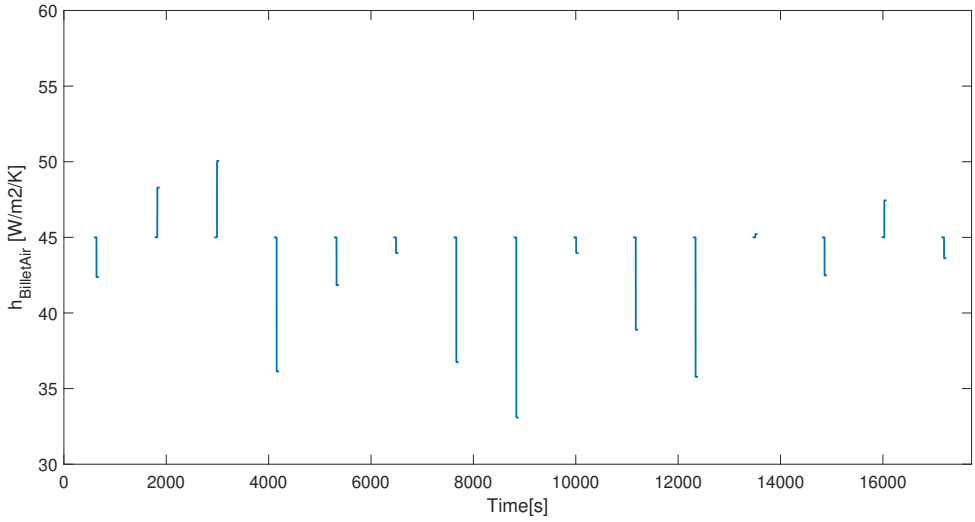

Figure 6.48: Estimated h_{billet} in transit with MHE with a longer data series and an initial value of $45\,\text{W/m}^2\text{K}$ for h_{billet}.

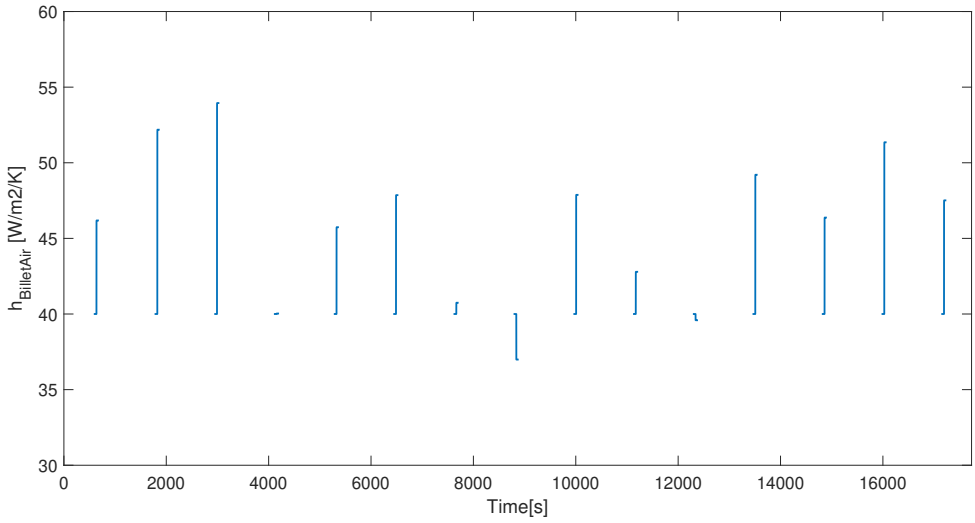

Figure 6.49: Estimated h_{billet} in transit with MHE with a longer data series and an initial value of $40\,\text{W/m}^2\text{K}$ for h_{billet}.

For the press both the temperatures in Figure 6.50 and parameters in 6.51 the MHE behaved similarly to the original data set. Temperature predictions were still accurate, and estimated parameter values were around 0.7 for $CF_{\text{reduction region}}$ and 80 s for τ_{die}. The configuration of the MHE was therefore deemed good in the press.

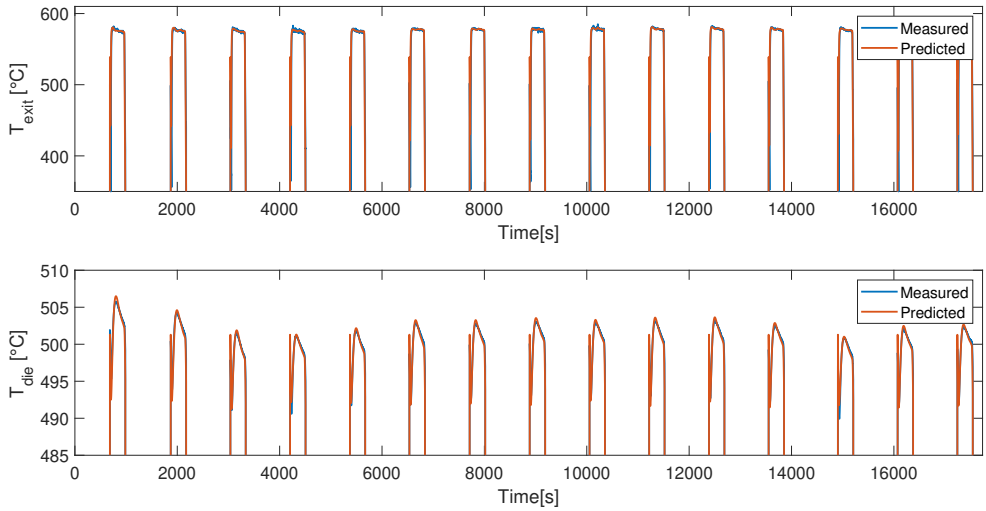

Figure 6.50: Measured and predicted values for T_{die} and T_{exit} during extrusion with MHE with a longer data series.

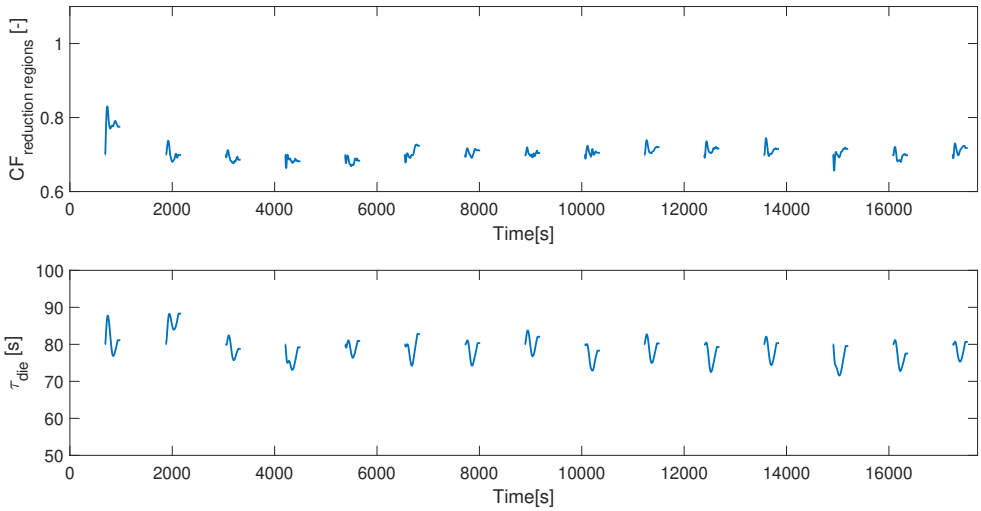

Figure 6.51: Estimated $CF_{\text{reduction region}}$ and τ_{die} in the extrusion press with MHE with a longer data series.

6.3.8 Simulation With Estimated Parameters

In this section the process was simulated with the new initial values for $CF_{\text{reduction regions}}$ and τ_{die}. As no new initial values were found in the heater or transit model these plots were identical to the ones shown in Section 6.3.1, and only the plot of the temperatures in the press was therefore included in this section. It is shown in Figure 6.52, and it shows significant improvement for T_{exit} while T_{die} had a small reduction in accuracy compared to Section 6.3.1. The new initial values nevertheless seemed to improve the behaviour of the press. With the old parameters the predicted values for T_{exit} were significantly higher than the measured ones, while T_{die} was quite accurate. The predictions for T_{exit} indicated that there was too much heat generation in the model, and the new estimate for $CF_{\text{reduction regions}}$, equal to 0.7, was lower than the original value of 1.0. This means the updated model generates less heat. Alone this would result in too low values for T_{die}, but it was compensated for by the increase in τ_{die} from 60 to 80. This increase meant the heat loss from the die itself was lower, increasing T_{die}. An important goal in the project was to be able to generate accurate predictions for T_{peak}. As the lower heat generation in the model using estimated parameter values gave better predictions for T_{exit}, it is also expected to have improved accuracy for T_{peak}.

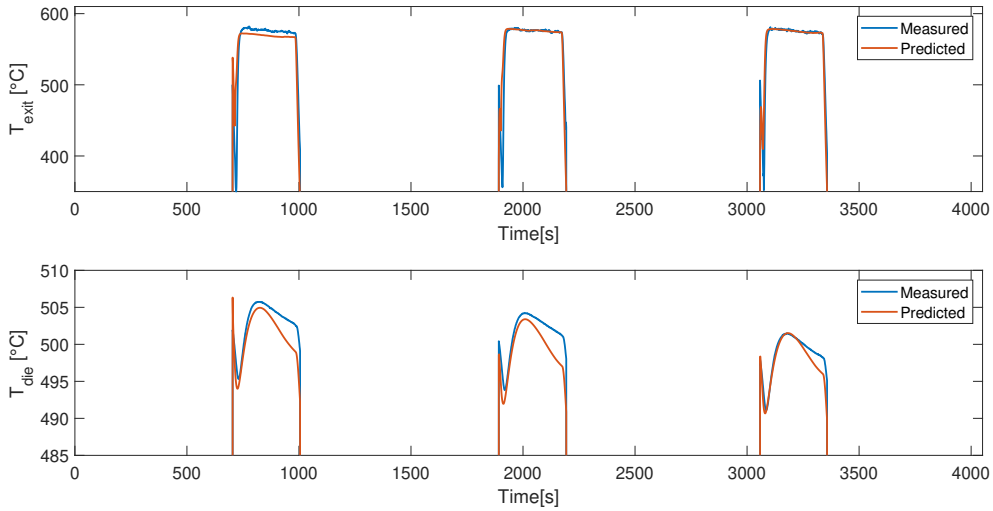

Figure 6.52: Measured and predicted values for T_{die} and T_{exit} during extrusion with estimated parameter values and without MHE.

6.4 Optimizing Ram Speed using Estimated Parameters

This section describes the results from solving the optimization problem formulated in Section 4.2, but now with the parameter values estimated in Section 6.3. The resulting values from T_{peak} and ram speed are shown in Figure 6.53, and the values for the temperature set points are the same as the ones used in Section 6.1. Figures showing the billet temperature during the process and heating coil activity are shown in Section A.2. The plot of T_{peak} showed good set point tracking, and the extrusion time was 248 s. This was significantly faster than the results using the original parameter values. The new ram speed was between approximately 3 mm/s and 4 mm/s, which is in the same range as the logged data from Hydro. This is an indication that the new model parameters, with less heat generation during extrusion, were a better fit for the real system, since its behaviour more resembled the logged data.

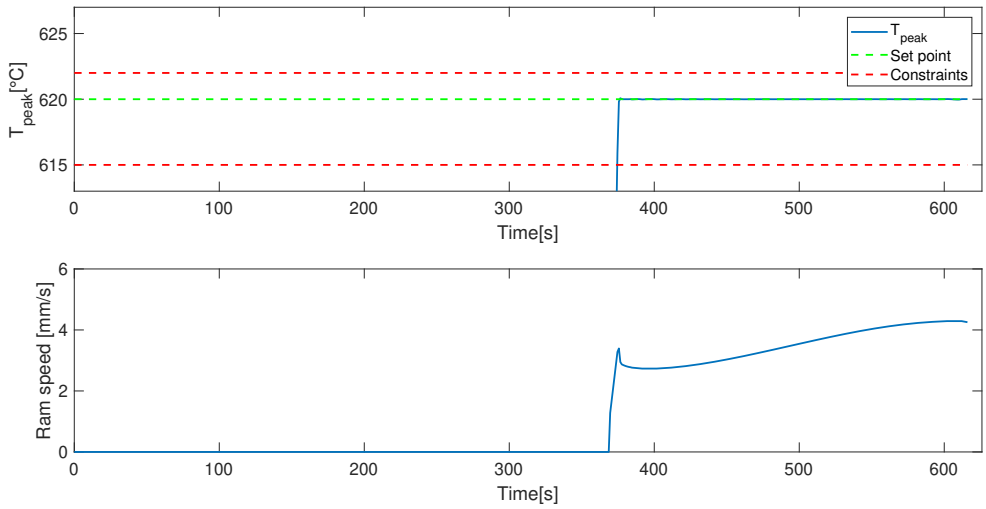

Figure 6.53: Optimized ram speed and T_{peak} with estimated parameter values.

6.5 Optimizing Ram Speed and Heating using Estimated Parameters

This section describes the results from solving the optimization problem formulated in Section 4.3 with the estimated parameter values from Section 6.3. Here, both the ram speed and the temperature set points in the heater were used as manipulated variables. The tunings used in the optimization were $q_1 = 15$ and $q_1 = 30$. The resulting values for T_{peak} and ram speed are shown in Figure 6.54, and the temperature set points are shown in Figure 6.55. Exact temperature values can also be found in Table 6.3. Figures showing the billet temperature during the process and heating coil activity are shown in Section A.4. Figure 6.54 shows excellent set point tracking for T_{peak}, and the time used in the extrusion press was 201 s. As for the optimization of only ram speed, this was faster than the optimization with original parameters. The ram speed was now higher than 4 mm/s for the entire extrusion cycle, except for the initial ramp up, and it was at the set point and maximum constraint of 5 mm/s at the end. The set points in the heater had a similar shape to the optimization with original parameters. It was warmer than before, and the gradient was lower, but it still had a slightly increasing gradient towards the end. Now, the temperature difference between coil 1 and 2 was 12 °C, between coil 2 and 3 it was 14 °C and between coil 3 and 4 it was 18 °C. The results show that significant improvement is possible from today's operation procedures. By reducing the temperature set points from between 530 °C and 485 °C to between 515 °C and 470 °C it was possible to increase the ram speed so that the extrusion time sunk from 300 s to 201 s. One third of the extrusion time could therefore possibly be removed by implementing the optimized heater set points and ram speed.

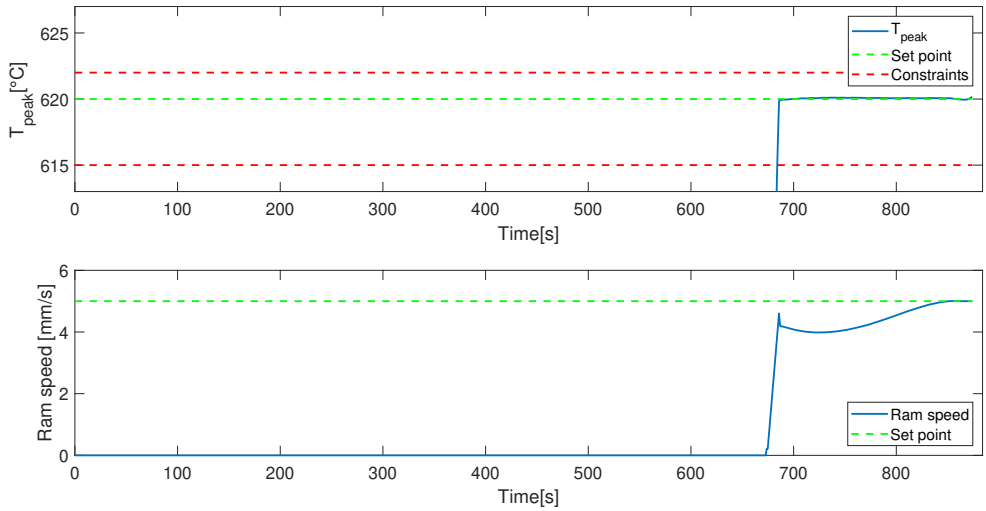

Figure 6.54: Optimized ram speed and T_{peak} with estimated parameter values from optimization of both ram speed and heating.

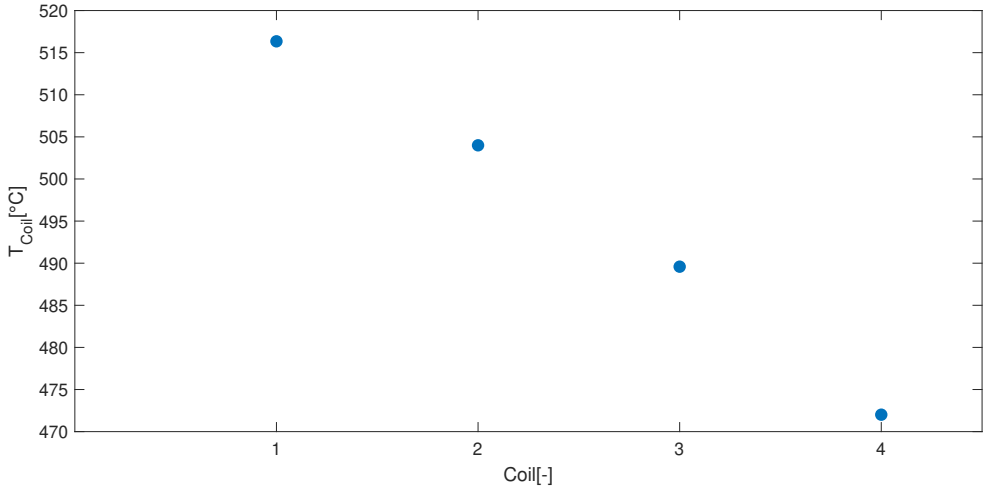

Figure 6.55: Optimized temperature set points in the heater for optimization using estimated parameter values.

Table 6.3: Heating coil set points from logged data and for optimizations with old and new parameter values.

Coil	Logged data [°C]	Old parameters [°C]	New parameters [°C]
1	530	466	516
2	513	443	504
3	494	419	490
4	485	387	472

7 Conclusions

In this project a complete model of an extrusion cycle for aluminium was created by combining existing models of a preheater, transit period and extrusion press. The existing models were made by the company Cybernetica and were first-principle models based on finite differences. The combined model was used in open loop dynamic optimization aimed at achieving good set point tracking for the temperature of the aluminium as it goes through its final shaping in the die (T_{peak}) and also minimizing the extrusion time. The results from the optimization showed that significant improvements in both set point tracking for T_{peak} and extrusion time are possible for the extrusion process. The results from Section 6.4 showed that very good set point tracking for T_{peak} was achievable by optimizing only the ram speed, and in Section 6.5 it was showed that optimizing the set points for the heating coils as well allowed for equally good values for T_{peak} while also reducing the extrusion time by 30%.

Parameter estimation was also implemented with the model. An investigation was made in to which parameters should be estimated and what their initial values should be by using moving horizon estimation (MHE) with measurements from Hydro. The results in Section 6.3 showed that the model struggled to fit the measurements in the heater. Some of this might have been due to inaccurate measurements. For example, the measurement of the temperature at the back end of the billet was deemed too inaccurate to use due to a bad fit to the model and information from Hydro that it might be faulty. For the other measurements the model mismatch was smaller but still significant for some, and the MHE was not able to improve it satisfactorily. The best results were achieved by estimating the heat transfer coefficients from the billet ends and heating coil bias, while leaving the correction factor for aluminium conductivity constant. As the fit was still not good assumptions used in the heater model, like that there is only heat loss from the ends of the billets, should be investigated again to see if the model fit can be improved. In the transit model the model predictions were good, but the estimated heat transfer coefficient varied a lot from billet to billet. This was most likely because there was only measurements at one point in time in the transit phase, which means parameter estimates become more uncertain. If one wants better estimates, measurements at more points in time per billet are required. In the extrusion press very good model predictions were achieved by estimation the correction factor for heat generated in regions of cross-sectional area reduction in the press and the time constant for a heat loss in the die. New initial values for these parameters were found to be 0.7 and 80 s respectively. The remaining parameters were left constant at their original initial values. A simulation with the updated parameter values without MHE showed showed improved performance compared to simulations with the original parameters. As a good fit in the extrusion press was considered most important, the MHE was deemed overall to perform well even though the predictions in the heater were not satisfactory. Comparisons of the results from optimizing only the ram speed before and after parameter estimation also showed that with the new parameter values the optimized process operated at a ram speed more similar to logged data. This is an indication that the updated parameters made the model describe the process more accurately, as the original parameter values resulted in a much lower ram speed.

8 Recommendations for further work

The optimizations of both ram speed and heating coil set points struggled with instability and were difficult to tune. They also took a long time to solve, often around 5 minutes. A reason for this might be that the software used to solve the optimization problems uses single shooting. This method is not well suited for highly nonlinear optimization problems with long prediction horizons, and the problems solved in this project are both. Another solving method, like for example multiple shooting or orthogonal collocation, could possibly improve both stability and performance.

The model proved not to be a good fit for measurements in the heater. This might be due to assumptions made in the model development, and if improved accuracy is desired one should retest them to see if they are good. One possible assumption to test is that there is only heat loss from the billet ends in the heater and not the rest of the surface.

The extrusion press studied in this project also has cooling available, but this degree of freedom was not utilized in this project. Using this in the optimization could possibly allow for even faster extrusion, as one might be able to run the extrusion press at maximum speed and do set point tracking for T_{peak} using the cooling instead.

There were too few temperature measurement points in time in the transit period to get accurate parameter estimates. To improve this, more measurements should be made by for example mounting a thermal imager on the transport mechanism for the billet. This would allow for continuous measurements of billet surface temperatures during transit.

References

[1] Alessandri, A., Baglietto, M., Battistelli, G., and Zavala, V. Advances in moving horizon estimation for nonlinear systems. *49th IEEE Conference on Decision and Control* (2010).

[2] Aukrust, T., and LaZghab, S. Thin shear boundary layers in flow of hot aluminium. *International Journal of Plasticity 16* (2000).

[3] Bastani, A. F., Aukrust, T., and Brandal, S. Study of isothermal extrusion of aluminum using finite element simulations. *Springer-Verlag France* (2010).

[4] Bastani, A. F., Aukrust, T., and Brandal, S. Optimisation of flow balance and isothermal extrusion of aluminium using finite-element simulations. *Journal of Materials Processing Technology* (2011).

[5] Bird, R. B., Stewart, W. E., and Lightfoot, E. N. *Transport phenomena*, 2nd ed. John Wiley & Sons, 2006.

[6] Foss, B., and Heirung, T. A. N. Merging optimization and control. *Technical report* (2016).

[7] Haseltine, E. L., and Rawlings, J. B. Critical evaluation of extended kalman filtering and moving-horizon estimation. *Industrial & Engineering Chemistry Research* (2005).

[8] Jakobsen, H. A. *Chemical Reactor Modeling*, 1st ed. Springer, 2008.

[9] Matamoros, C. F. C. Modeling and control for the isothermal extrusion of aluminium. *Swiss Federal Institute of Technology Zurich* (1999).

[10] Nocedal, J., and Wright, S. J. *Numerical Optimization*, 2nd ed. Springer, 2006.

[11] Pedersen, B. aluminium. `https://snl.no/aluminium`. Accessed on 10.10.2021.

[12] Rao, C. V., Rawlings, J. B., and Mayne, D. Q. Constrained state estimation for nonlinear discrete-time systems: Stability and moving horizon approximations. *IEEE TRANSACTIONS ON AUTOMATIC CONTROL, VOL. 48, NO. 2* (2003).

[13] Schei, T. S. On-line estimation for process control and optimization applications. *Journal of Process Control 18* (2008).

[14] Cybernetica. Technology model predictive control. `https://cybernetica.no/technology/model-predictive-control/`. Accessed on 23.11.2021.

[15] Encyclopedia of Mathematics. Finite-difference calculus. `https://encyclopediaofmath.org/index.php?title=Finite-difference_calculus`. Accessed on 22.11.2021.

[16] Hydro. Micro-channel tubes. `https://www.hydro.com/en/aluminium/products/precision-tubes/micro-channel-tubes/`. Accessed on 02.12.2021.

[17] Scholarpedia. Stiff systems. `http://www.scholarpedia.org/article/Stiff_systems`. Accessed on 22.11.2021.

[18] The Research Council of Norway. Extrutec - high precision extrusion temperature control through digital technology. `https://prosjektbanken.forskningsradet.no/en/project/FORISS/313919?Kilde=FORISS&distribution=Ar&chart=bar&calcType=funding&Sprak=no&sortBy=date&sortOrder=desc&resultCount=30&offset=120&TemaEmne.2=IKT-n%C3%A6ringen`. Accessed on 10.10.2021.

A Optimization Results

In this section results from the optimizations not included in Section 6 are shown.

A.1 Optimized Ram Speed using Original Parameters

Figure A.1 and A.2 show billet temperature and coil status during extrusion for the optimization of ram speed using original parameter values.

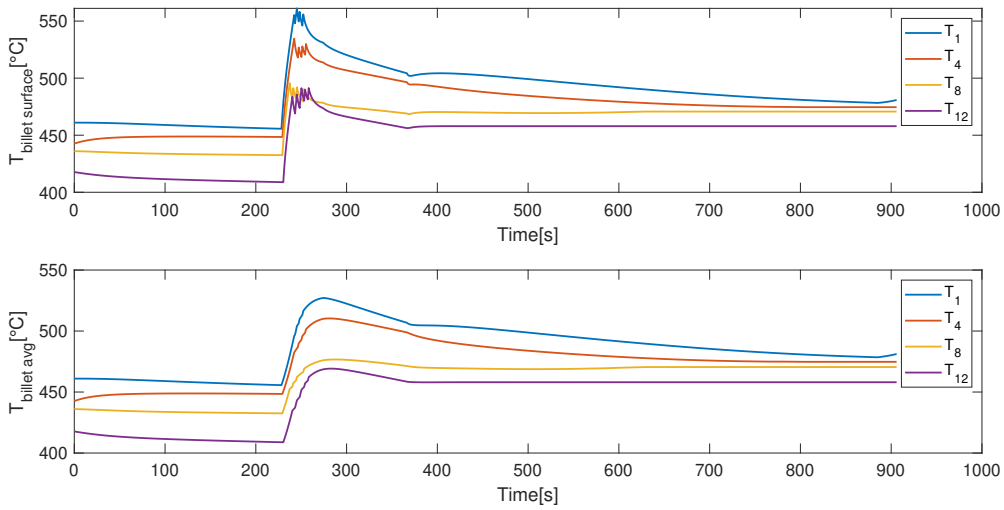

Figure A.1: Surface and radial average billet temperature during extrusion for the optimization of ram speed using original parameter values.

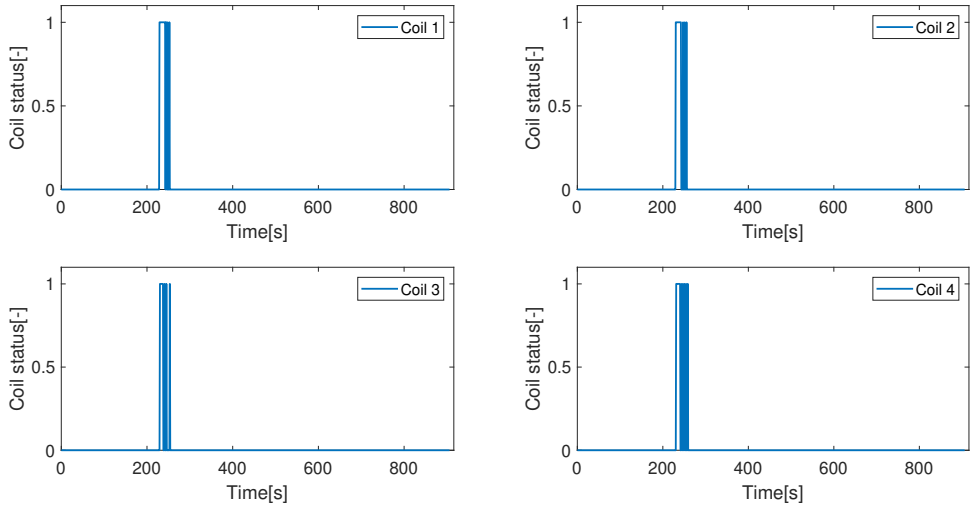

Figure A.2: Heating coil status during extrusion for the optimization of ram speed using original parameter values.

A.2 Optimized Ram Speed using Estimated Parameters

Figure A.3 and A.4 show billet temperature and coil status during extrusion for the optimization of ram speed using estimated parameter values.

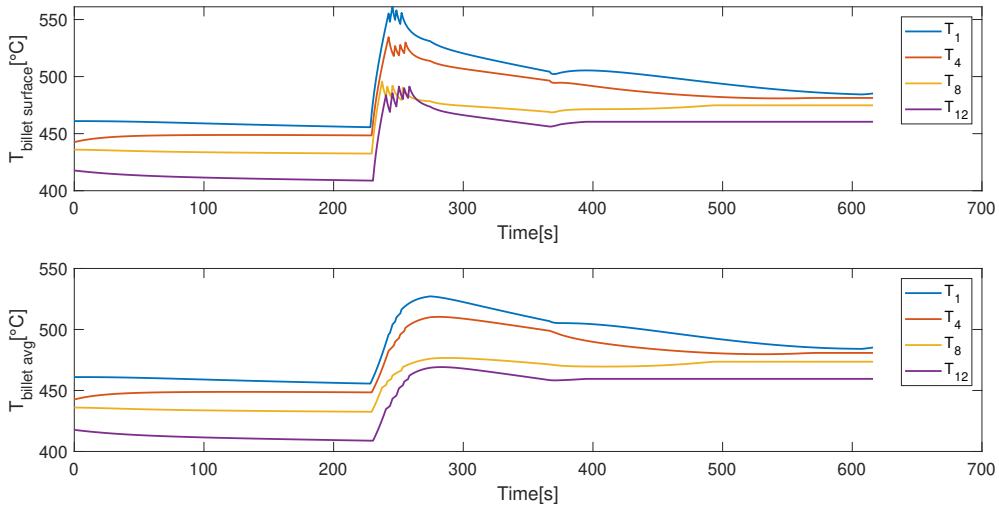

Figure A.3: Surface and radial average billet temperature during extrusion for the optimization of ram speed using estimated parameter values.

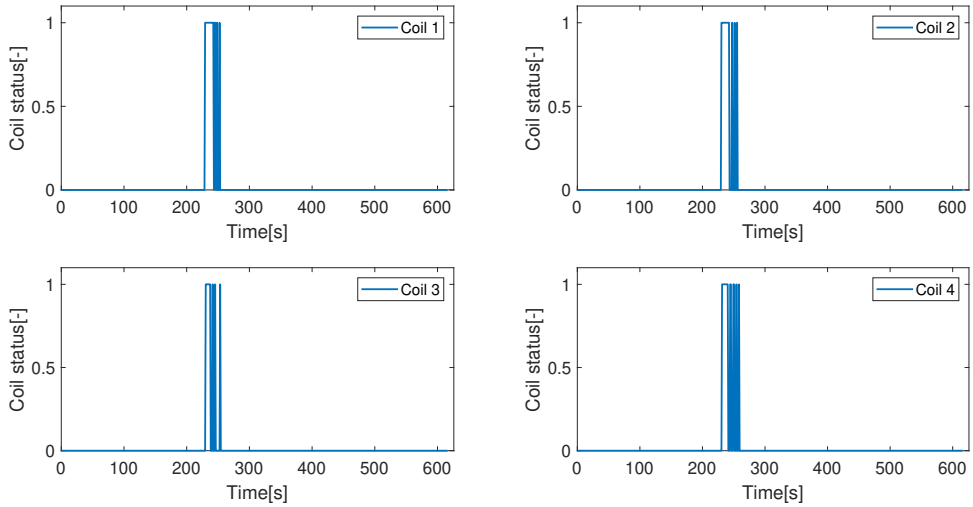

Figure A.4: Heating coil status during extrusion for the optimization of ram speed using estimated parameter values.

A.3 Optimized Ram Speed and Heating using Original Parameters

Figure A.5 and A.6 show billet temperature and coil status during extrusion for the optimization of ram speed and heating using original parameter values.

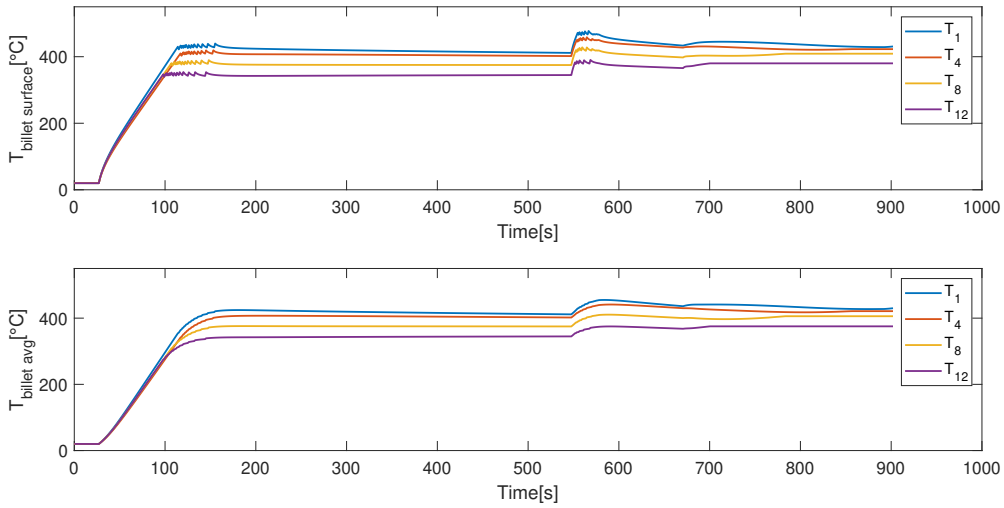

Figure A.5: Surface and radial average billet temperature during extrusion for the optimization of ram speed and heating using original parameter values.

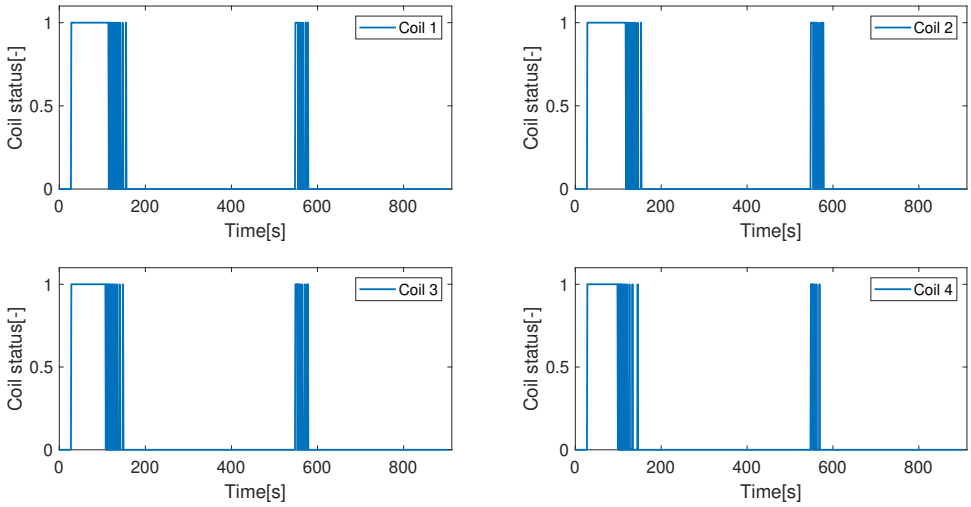

Figure A.6: Heating coil status during extrusion for the optimization of ram speed and heating using original parameter values.

A.4 Optimized Ram Speed and Heating using Estimated Parameters

Figure A.7 and A.8 show billet temperature and coil status during extrusion for the optimization of ram speed and heating using estimated parameter values.

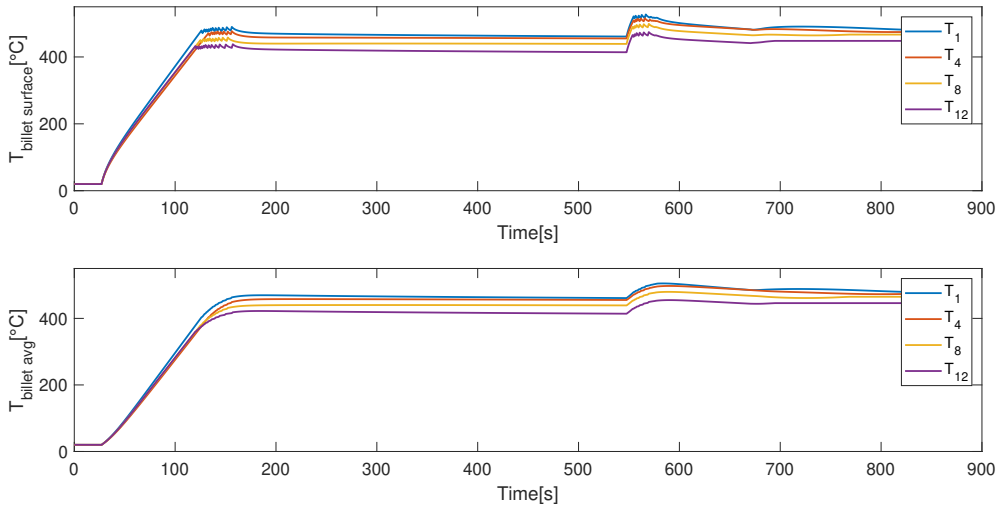

Figure A.7: Surface and radial average billet temperature during extrusion for the optimization of ram speed and heating using estimated parameter values.

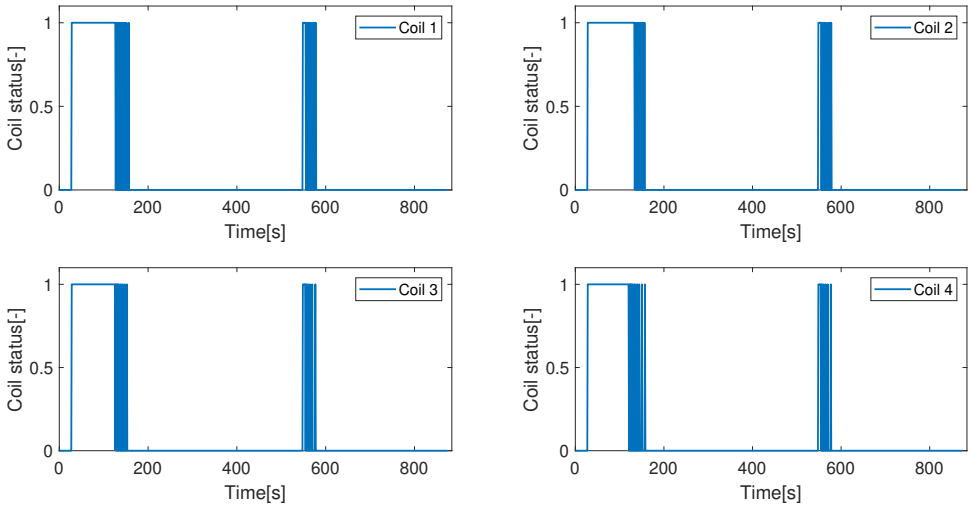

Figure A.8: Heating coil status during extrusion for the optimization of ram speed and heating using estimated parameter values.

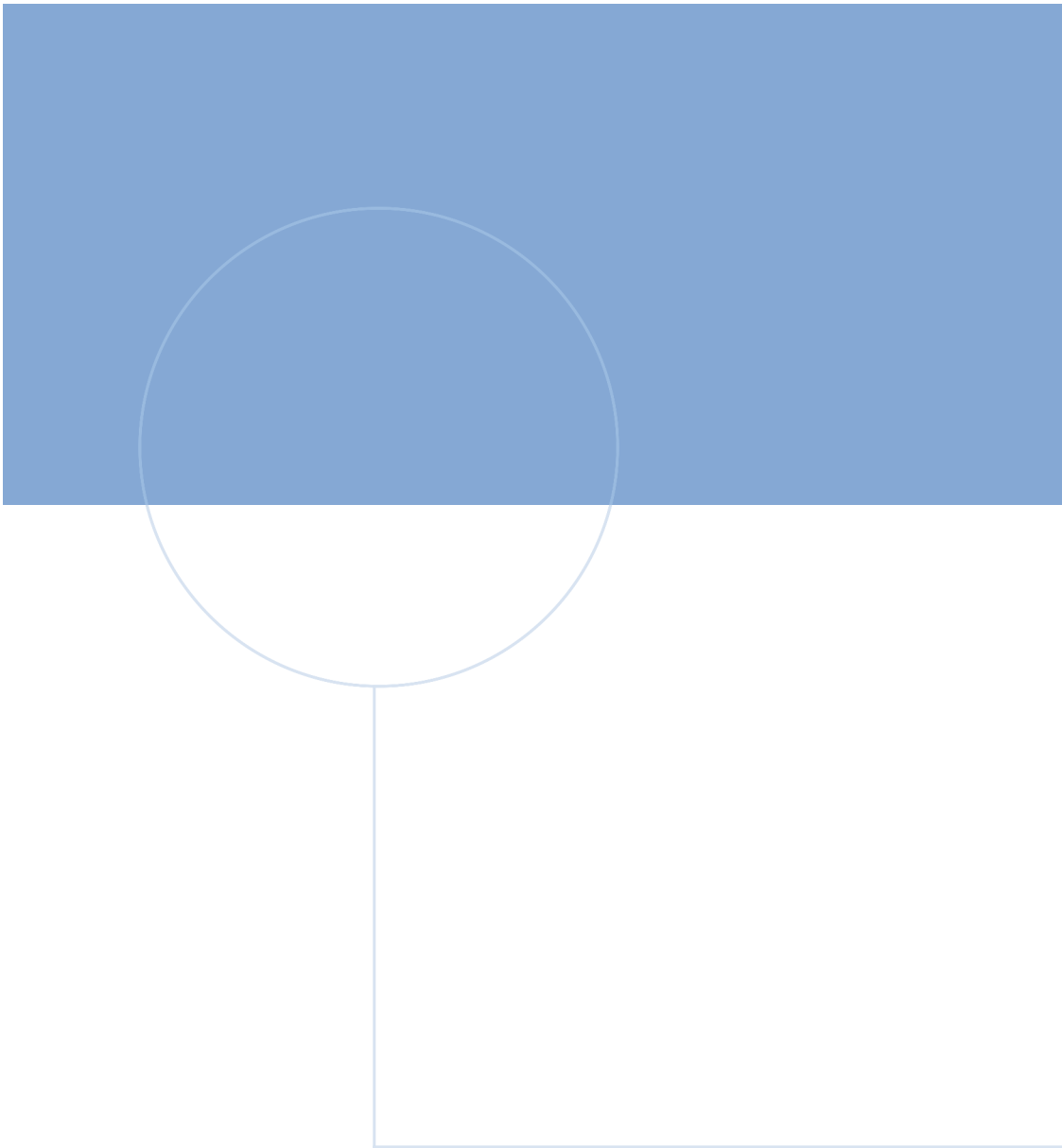

NTNU

Kunnskap for en bedre verden